International Journal of
Molecular Sciences

MDPI

Article

Ginkgo biloba Flower Extract Accelerates the Wound Healing in Diabetic Rats by Inhibiting Inflammation and Ferroptosis

Xin Sun [1,2], Ruihong Li [2], Yingying Xu [1,2], Yuying Wang [2], Ziming Xia [2], Ying Tian [2], Guangjie Zhang [2], Sifan Liu [2], Min Li [2,*] and Shuchen Liu [1,2,*]

[1] School of Pharmacy, Anhui Medical University, Hefei 230032, China; sunx0102@163.com (X.S.); 15665648396@163.com (Y.X.)
[2] Academy of Military Medical Sciences, Beijing 100850, China; lrh1217021@163.com (R.L.); wangyuying0829@163.com (Y.W.); zmxia22@163.com (Z.X.); tianying1977@126.com (Y.T.); zhanggj410@sina.com (G.Z.); 18146539471@163.com (S.L.)
* Correspondence: limin82057@163.com (M.L.); liusc118@163.com (S.L.)

Abstract

Diabetic wounds are a common complication of diabetes mellitus (DM), with healing often impaired by ferroptosis and persistent inflammation. This study investigated the effects of *Ginkgo biloba* flower extract (GBF) on diabetic wound healing by focusing on inflammation and ferroptosis. Chemical composition analysis identified 123 compounds in GBF containing 73 active ingredients of flavonoids and 12 terpenoids. In vivo, GBF treatment significantly accelerated the wound healing process in diabetic rats, and GBF promoted epithelial regeneration and collagen deposition by increasing the expression of CD31 and VEGF. It also enhanced the formation of new blood vessels. Mechanistically, GBF could inhibit the inflammatory response by reducing the levels of tumor necrosis factor-α (TNF-α) and interleukin-6 (IL-6), and inhibit the oxidative stress-induced ferroptosis by increasing the levels of glutathione (GSH) and glutathione peroxidase 4 (GPX4). Proteomics analysis further confirmed its regulatory effects on inflammation and iron metabolism pathways. In vitro, GBF promoted the survival and migration of rat skin fibroblasts (RS1) while reducing the levels of reactive oxygen species (ROS) and Fe^{2+} in erastin-induced ferroptosis cells. In conclusion, GBF promotes diabetic wound healing by inhibiting ferroptosis and inflammation.

Keywords: diabetic wound healing; *Ginkgo biloba* flower; ferroptosis; inflammation

Check for updates

Academic Editor: Simona Martinotti

Received: 15 May 2026
Revised: 22 June 2026
Accepted: 25 June 2026
Published: 26 June 2026

Copyright: © 2026 by the authors. Licensee MDPI, Basel, Switzerland. This article is an open access article distributed under the terms and conditions of the Creative Commons Attribution (CC BY) license.

1. Introduction

Diabetes mellitus (DM) is a global chronic metabolic disorder. Recent epidemiological projections indicate that the global prevalence of diabetes will surge from 529 million in 2021 to over 1.3 billion by 2050 [1]. DM has many serious complications, among which diabetic kidney disease (DKD), one of the types of chronic kidney disease (CKD), is one of the most serious complications. In DKD, a high-glucose environment induces metabolic reprogramming of glucose, lipid and protein in proximal renal tubular epithelial cells, leading to volume overload, oxidative stress and mitochondrial dysfunction [2]. During this process, renal tubular epithelial cells undergo epithelial–mesenchymal transition (EMT) and obtain a mesenchymal fibroblast-like phenotype, which directly promotes tubular atrophy, interstitial inflammation and extracellular matrix deposition [3]. In addition, the zinc finger protein YY1 induces a positive feedback loop by up-regulating hypoxia-inducible factor-1 alpha (HIF-1α) and promoting the excessive production of mitochondrial reactive

oxygen species (mROS), further aggravating the proliferation and sclerosis of glomerular mesangial cells [4]. The core pathological process in the progression of CKD to end-stage renal disease is renal fibrosis, and its molecular mechanism involves ferroptosis, oxidative stress, inflammatory response, and complex interactions of multiple signaling pathways, especially in the context of DM [5]. Diabetic wounds are another common and serious complication of DM; these wounds are strongly associated with extremely high rates of lower limb amputation and mortality. A prospective cohort study showed that the cumulative incidence of lower limb amputation within 12 months after the first occurrence of diabetic wounds was 24.2%, while the 12-month mortality rate was as high as 21.6% [6]. A recent population-based study showed a prevalence of 4.6% and an annual incidence of 2.1%, which further confirmed its high mortality rate, with a 5-year mortality rate of about 64% in patients with infectious diabetic wounds [7]. The multifactorial pathophysiological mechanisms of diabetic wounds, including chronic hyperglycemia, oxidative stress, persistent inflammation, impaired angiogenesis, and altered cellular function, further aggravate these harms [8]. Despite the devastating consequences of diabetic wounds described above, current therapeutic options remain limited. Standard care includes debridement, infection control, offloading, and revascularization when indicated, but these approaches often fail to achieve timely healing in a significant proportion of patients [9,10]. Effective strategies to accelerate the healing of diabetic wounds, control infection, prevent tissue necrosis, and reduce amputation risk remain unmet clinical and scientific challenges, primarily due to the incomplete elucidation of diabetic wound pathogenesis and the lack of targeted therapeutics [11].

Accumulating evidence highlights multiple pathogenic mechanisms underlying diabetic wounds, including persistent inflammation, ferroptosis, oxidative stress, and immune dysregulation. The chronic hyperglycemic microenvironment in diabetic wounds drives sustained inflammatory cell infiltration, perpetuating a state of chronic inflammation [12,13]. This has a similar pathogenesis to DKD. As a chronic refractory wound, diabetic wounds are characterized by a persistent high-glucose microenvironment that drives the accumulation of neutrophils and macrophages, and the continuous release of tumor necrosis factor-α (TNF-α) and interleukin-6 (IL-6). These abnormalities maintain the wound in a chronic inflammatory state, thereby preventing its transition to the proliferative phase [12,13]. Ferroptosis, an iron-dependent, non-apoptotic form of regulated cell death, is characterized by elevated intracellular Fe^{2+} levels, excessive reactive oxygen species (ROS) production, diminished glutathione peroxidase 4 (GPX4) activity, and lipid peroxide accumulation, ultimately leading to cell demise [14,15]. Emerging studies have identified iron metabolism as a key regulator of wound healing [16], and ferroptosis has been documented in diabetic wounds [17–19]. The occurrence of ferroptosis impairs the viability of skin fibroblasts and vascular endothelial cells, thereby delaying diabetic wound healing [20,21]. A long-term high-glucose environment in diabetic wounds can also lead to oxidative stress, leading to the depletion of glutathione (GSH), the precursor of GPX4 synthesis, resulting in the accumulation of ROS, which activates lipid peroxidation and causes ferroptosis [22]. In addition, oxidative stress can activate inflammatory pathways such as NF-κB, up-regulate the expression of pro-inflammatory factors, and aggravate local chronic inflammatory response [23]. The vicious cycle of "oxidative stress–inflammation–ferroptosis" seriously inhibits the process of wound repair. Thus, targeting inflammation and ferroptosis represents a promising therapeutic approach for diabetic wound management.

Natural products, renowned for their structural diversity and multi-target bioactivity, serve as invaluable sources for drug discovery. At present, some progress has been made in the research of natural products in the field of diabetic wound healing. Many studies have shown that natural bioactive compounds such as resveratrol and ginsenoside can promote

diabetic wound healing by regulating programmed cell death pathways including apoptosis and ferroptosis [24]. Extracts of natural products such as quercetin, curcumin, and paeoniflorin act through antioxidant, antibacterial, anti-inflammatory, and pro-angiogenic mechanisms [25]. Current research on natural products mostly focuses on a single pathway, while the disorder of diabetic wound healing is a complex result of the interaction of multiple pathological factors [26]. Therefore, it is of great significance to clarify the multi-target regulatory mechanism of inflammation and ferroptosis for diabetic wound healing. *Ginkgo biloba* L, a "living fossil" and the sole surviving species of the Ginkgophyta division, is rich in bioactive components such as flavonoids and terpene lactones, exhibiting pharmacological effects including blood circulation promotion and lipid lowering [27]. Clinically, *Ginkgo biloba* L are widely used for cardiovascular and cerebrovascular protection [28]. At present, the pharmacological properties of *Ginkgo biloba* leaves have been extensively studied, but the research on the male flower of *Ginkgo biloba* flower extract (GBF) is still in its infancy [29]. Our previous study showed that the contents of flavonoids (1.42 times higher), amino acids (15.7 times higher) and fatty acids (7.4 times higher) in GBF were significantly higher than those in *Ginkgo biloba* leaf extract. Of the 73 identified flavonoids, 57 were found to be more abundant in GBF [29,30]. These results suggest that GBF may be a superior choice for the source of bioactive compounds compared to the conventionally used *Ginkgo biloba* leaf extract. Notably, GBF showed superior anti-ferroptosis activity in erastin-induced PC12 cells and exerted stronger anti-inflammatory effects through bilobetin and isoginkgetin [29,31]. Therefore, GBF had a stronger inhibitory effect on inflammation and ferroptosis than *Ginkgo biloba* leaf extract. However, the therapeutic potential of GBF in diabetic wound healing has not been fully investigated. Therefore, this research chose to focus on inflammation and ferroptosis to investigate the effect of GBF on diabetic wound healing in the expectation of discovering a novel natural product candidate with potential in diabetic wound treatment.

2. Results

2.1. Qualitative Analysis of the Total Chemical Composition of GBF

The mass spectrometry data collected were processed using the following methods: Progenesis QI 3.0 software (Waters Corp, Mlford, MA, USA) was used. The operation steps were as follows: import raw data, peak extraction and deconvolution processing. The reference material database (TCM Pro 2.0, Beijing Hexin Technology, Beijin, China) and theoretical databases (based on the literature and public databases) were searched. Based on the retention time error of reference materials, mass error of parent ions, matching of secondary fragments, isotope distribution, peak intensity and other factors, the identification results were comprehensively evaluated and analyzed in multiple dimensions, and the final results were obtained. The base peak ion chromatograph (BPI) of GBF is shown in Figure 1. Finally, 123 compounds were identified in GBF (Table 1), including 73 flavonoids, 12 terpenoids, 10 phenolic acids, six alkaloids and five phenylpropanoids. Other chemical classes include anthraquinones, fatty acids, amino acids, purines, and alkaloids.

Table 1. Analysis and identification of chemical constituents in GBF.

No.	tR/ (min)	Name	Formula	*m/z*	Expected *m/z*	Adducts	Reference
1	0.91	Stachydrine	$C_7H_{13}NO_2$	144.1019	144.1019	M + H	[32]
2	1.27	Nicotinamide	$C_6H_6N_2O$	123.0557	123.0557	M + H	
3	1.50	Dl-isoleucine	$C_6H_{13}NO_2$	132.1020	132.1019	M + H	[33]
4	1.61	α-arbutin	$C_{12}H_{16}O_7$	317.0879	317.0878	M-H, M + FA-H	[34]

Table 1. *Cont.*

No.	tR/ (min)	Name	Formula	*m/z*	Expected *m/z*	Adducts	Reference
5	2.34	Hordenine	$C_{10}H_{15}NO$	166.1226	166.1227	M + H	[35]
6	2.53	4-hydroxybenzoic acid	$C_7H_6O_3$	156.0654	156.0654	M + NH4	[36]
7	2.68	4-methoxypyridoxine	$C_9H_{13}NO_3$	184.0968	184.0968	M + H	[37]
8	3.14	3-(4-hydroxy-3-methoxyphenyl) propane-1,2-diol	$C_{10}H_{14}O_4$	181.0858	181.0858	M + H-H_2O	[36]
9	3.40	Cardiospermin	$C_{11}H_{17}NO_7$	274.0935	274.0932	M-H	[38]
10	4.02	Dl-pantothenic acid	$C_9H_{17}NO_5$	220.1177	220.1180	M + H-H_2O, M + H, M + Na	[39]
11	4.27	6-hydroxykynurenate	$C_{10}H_7NO_4$	206.0446	206.0448	M + H	[40]
12	4.65	Geniposidic acid	$C_{16}H_{22}O_{10}$	373.1144	373.1140	M-H	[41]
13	5.07	Neochlorogenic acid	$C_{16}H_{18}O_9$	353.0883	353.0878	M-H	[36]
14	5.12	(_)-epigallocatechin-(4beta-> 8)-(_)-epicatechin	$C_{30}H_{26}O_{13}$	593.1311	593.1300	M-H	[42]
15	5.46	3,4-dihydroxybenzaldehyde	$C_7H_6O_3$	139.0389	139.0390	M + H	[43]
16	5.67	Esculin	$C_{15}H_{16}O_9$	339.0723	339.0721	M-H	[36]
17	6.00	Bergenin	$C_{14}H_{16}O_9$	327.0725	327.0721	M-H	[44]
18	6.16	Hypaphorine	$C_{14}H_{18}N_2O_2$	247.1437	247.1441	M + H	[45]
19	6.36	Quercetin_3-o-rhamnoside_7-o-(6-feruloylglucosyl-(1–3)-rhamnoside)	$C_{33}H_{40}O_{22}$	787.1951	787.1938	M-H	
20	6.44	Isorhamnetin_3-arabinoglucoside	$C_{27}H_{30}O_{16}$	611.1599	611.1607	M + H	[43]
21	6.98	Esculetin	$C_9H_6O_4$	179.0337	179.0339	M + H	[36]
22	7.06	3,4,4a,5,6,7-hexahydro_1,1,4a-trimethyl-2(1 h)-naphthalenone	$C_{13}H_{20}O$	193.1585	193.1587	M + H	[46]
23	7.30	Quercetin-3-o-beta-d-glucosyl-(1–2)-alpha-l-rhamnoside	$C_{27}H_{30}O_{17}$	625.1417	625.1410	M-H	[37]
24	7.79	Aromadendrin	$C_{15}H_{12}O_6$	289.0700	289.0707	M + H-H_2O, M + H	[47]
25	7.96	(_)-epicatechin	$C_{15}H_{14}O_6$	335.0777	335.0772	M-H, M + FA-H	[48]
26	8.08	Sinapine thiocyanate	$C_{16}H_{24}NO_5$+	310.1645	310.1649	M + H	[49]
27	8.22	Isovanillic acid	$C_8H_8O_4$	169.0493	169.0496	M + H	[50]
28	8.45	Kaempferol_3-o-glucosy l (1–2) rhamnoside	$C_{27}H_{30}O_{15}$	593.1518	593.1512	M-H	[51]
29	9.34	Neoisorutin	$C_{27}H_{30}O_{16}$	611.1598	611.1607	M + H, M + Na, 2 M + H	[52]
30	9.44	Isorhamnetin_3-o-rutinoside	$C_{28}H_{32}O_{16}$	623.1622	623.1617	M-H	[36]
31	9.46	Pinoresinol diglucoside	$C_{32}H_{42}O_{16}$	727.2467	727.2455	M-H, M + FA-H	[36]
32	9.47	Myricetin	$C_{15}H_{10}O_8$	319.0442	319.0449	M + H	[53]
33	9.62	Isorhamnetin3-o-beta-D-glucopyranosyl-(1–2)-alpha-l-rhamnopyranoside	$C_{28}H_{32}O_{16}$	625.1754	625.1763	M + H-H_2O, M + H	[36]
34	9.96	Eucarvone	$C_{10}H_{14}O$	151.1116	151.1118	M + H	[50]
35	10.19	Secoisolariciresinol diglucoside	$C_{32}H_{46}O_{16}$	731.2788	731.2768	M-H, M + FA-H	[54]
36	10.35	Typhaneoside	$C_{34}H_{42}O_{20}$	769.2207	769.2197	M-H, M + FA-H	[51]
37	10.37	Isorhamnetin-3-O-rutinoside	$C_{28}H_{32}O_{16}$	625.1754	625.1753	M+H	
38	10.41	Bilobalide	$C_{15}H_{18}O_8$	325.0928	325.0929	M-H	[36]
39	10.48	Rutin	$C_{27}H_{30}O_{16}$	609.1464	609.1461	M-H	[36]
40	10.55	Quercetin_3-o-rhamnopyranoside	$C_{21}H_{20}O_{11}$	447.0934	447.0933	M-H	[36]

Table 1. *Cont.*

No.	tR/ (min)	Name	Formula	*m/z*	Expected *m/z*	Adducts	Reference
41	10.55	Quercetin 3-o-alpha-l-[6í-p-coumaroyl-beta-D-Glucopyranosyl-(1-> 2)-rhamnopyranoside]-7-o-beta-d-glucopyranoside	$C_{42}H_{46}O_{23}$	917.2373	917.2357	M-H	[36]
42	10.69	Kaempferol 3-o-alpha-l-rhamnopyranosyl(1-> 6)-beta-d-galactopyranoside	$C_{27}H_{30}O_{15}$	595.1647	595.1658	M + H, M + Na, 2 M + H	[36]
43	10.70	Kaempferol 3-o-rhamnoside	$C_{21}H_{20}O_{10}$	431.0982	431.0984	M-H	[54]
44	10.74	Kaempferol 3-o-alpha-l-[6í-p-coumaroyl-beta-D-Glucopyranosyl-(1-> 2)-rhamnopyranoside]-7-o-beta-d-glucopyranoside	$C_{42}H_{46}O_{22}$	901.2424	901.2408	M-H	[36]
45	10.82	Hyperoside	$C_{21}H_{20}O_{12}$	465.1020	465.1028	M + H, M + Na	[55]
46	10.96	Ginkgolid j	$C_{20}H_{24}O_{10}$	469.1351	469.1352	M-H, M + FA-H	[56]
47	11.01	Laricitrin	$C_{16}H_{12}O_8$	333.0596	333.0605	M + H	[57]
48	11.23	Ginkgolide c	$C_{20}H_{24}O_{11}$	439.1247	439.1246	M-H, M + FA-H	[36]
49	11.25	Gibberellic acid	$C_{19}H_{22}O_6$	347.1481	347.1489	M + H-H_2O, M + H	[41]
50	11.29	Isoquercitrin	$C_{21}H_{20}O_{12}$	463.0887	463.0882	M-H	[36]
51	11.45	Tricetin	$C_{15}H_{10}O_7$	303.0492	303.0500	M + H	[58]
52	11.58	Cynaroside	$C_{21}H_{20}O_{11}$	449.1069	449.1079	M + H	[59]
53	11.58	Nicotiflorin	$C_{27}H_{30}O_{15}$	593.1512	593.1512	M-H	[36]
54	11.69	Cosmetin	$C_{21}H_{20}O_{10}$	431.0985	431.0984	M-H	[36]
55	11.71	Perlolyrine	$C_{16}H_{12}N_2O_2$	265.0966	265.0972	M + H	[57]
56	11.88	(e)-4-(4-hydroxy-2,6,6-trimethylcyclohexen_1-yl) but-3-en-2-one	$C_{13}H_{20}O_2$	209.1531	209.1536	M + H	
57	11.92	Isorhamnetin-3-o-neohespeidoside	$C_{28}H_{32}O_{16}$	625.1749	625.1763	M + H, M + Na, 2 M + H	[36]
58	11.92	Tectoridin	$C_{22}H_{22}O_{11}$	463.1224	463.1235	M + H	[60]
59	11.94	Astragalin	$C_{21}H_{20}O_{11}$	449.1069	449.1079	M + H, M + Na	[36]
60	12.09	Syringetin_3-rutinoside	$C_{29}H_{34}O_{17}$	653.1730	653.1723	M-H, M + FA-H	
61	12.29	Sophoricoside	$C_{21}H_{20}O_{10}$	433.1121	433.1130	M + H, 2 M + H	[61]
62	12.31	Isorhamnetin 3-galactoside	$C_{22}H_{22}O_{12}$	477.1038	477.1038	M-H	[62]
63	12.48	Dihydroalangionoside A	$C_{19}H_{36}O_8$	392.2402	375.2369	M + H-H_2O, M +	[63]
64	12.53	Kaempferol 3-arabofuranoside	$C_{20}H_{18}O_{10}$	417.0830	417.0827	M-H	[61]
65	12.60	Hesperidin	$C_{28}H_{34}O_{15}$	609.1830	609.1825	M-H	[64]
66	12.81	Thermopsoside	$C_{22}H_{22}O_{11}$	463.1226	463.1235	M + H, 2 M + H	[65]
67	12.89	Trifolin	$C_{21}H_{20}O_{11}$	449.1070	449.1079	M + H	[66]
68	13.09	Rhoifolin	$C_{27}H_{30}O_{14}$	577.1571	577.1563	M-H	[67]
69	13.34	Quercetin 3-o-alpha-l-[6í-p-coumaroyl-beta-D-glucopyranosyl-(1-> 2)-rhamnopyranoside]	$C_{36}H_{36}O_{18}$	755.1834	755.1829	M-H	[36]
70	13.65	Coniferin	$C_{16}H_{22}O_8$	387.1302	387.1302	M + FA-H	[68]
71	13.76	Bilobanone	$C_{15}H_{20}O_2$	215.1427	215.1430	M + H-2H_2O	[69]
72	14.17	Daidzein	$C_{15}H_{10}O_4$	255.0644	255.0652	M + H	[61]

Table 1. *Cont.*

No.	tR/ (min)	Name	Formula	*m/z*	Expected *m/z*	Adducts	Reference
73	14.32	Kaempferol 3-o-alpha-l-[6í-p-coumaroyl-beta-D-glucopyranosyl-(1-> 2)-rhamnopyranoside]	$C_{36}H_{36}O_{17}$	739.1887	739.1880	M-H	[36]
74	14.41	Isorhamnetin 3-o-a-l-[6,-p-coumaroyl-b-D-glucopyranosyl-(1,2)-rhamnopyranoside]	$C_{37}H_{38}O_{18}$	769.1993	769.1985	M-H, M + FA-H	[61]
75	14.43	Alangionoside A	$C_{19}H_{34}O_8$	373.2213	373.2213	M + H-H_2O	[70]
76	14.59	Ginkgolid a	$C_{20}H_{24}O_9$	409.1484	409.1493	M + H-2H_2O	[36]
77	14.63	Ginkgolide b	$C_{20}H_{24}O_{10}$	423.1299	423.1297	M-H, M + FA-H	[36]
78	14.8	Dihydrodendranthemoside A	$C_{19}H_{36}O_8$	415.2321	415.2321	M + Na	[71]
79	15.01	Luteolin	$C_{15}H_{10}O_6$	285.0405	285.0404	M-H	[36]
80	15.28	Andrographolide	$C_{20}H_{30}O_5$	349.2023	349.2020	M-H	[72]
81	15.42	Tiliroside	$C_{30}H_{26}O_{13}$	593.1310	593.1300	M-H	[73]
82	15.67	Calycosin	$C_{16}H_{12}O_5$	283.0612	283.0612	M-H	[74]
83	16.32	Trans-caffeic acid	$C_9H_8O_4$	163.0386	163.0386	M + H-H_2O	[61]
84	16.50	Naringenin	$C_{15}H_{12}O_5$	271.0611	271.0612	M-H	[75]
85	16.72	Silibinin	$C_{25}H_{22}O_{10}$	481.1142	481.1140	M-H	[76]
86	16.76	Genistein	$C_{15}H_{10}O_5$	271.0593	271.0601	M + H	[74]
87	16.93	Hesperetin	$C_{16}H_{14}O_6$	301.0715	301.0717	M-H	[70]
88	16.94	4,4,-dihydroxy-3,3,-imino-di-benzoic acid	$C_{14}H_{11}NO_6$	289.0594	289.0594	M + H	[60]
89	16.97	Kaempferol	$C_{15}H_{10}O_6$	285.0403	285.0404	M-H	[36]
90	17.20	Diosmetin	$C_{16}H_{12}O_6$	301.0699	301.0707	M + H	[77]
91	17.36	Isorhamnetin	$C_{16}H_{12}O_7$	317.0648	317.0648	M + H	[36]
92	17.53	(1ar,4as,7r,7ar,7br)-1,1,7-trimethyl_4-methylidenedecahydro-1 h-cyclopropa(e)azulen_7-ol	$C_{15}H_{24}O$	221.1895	221.1900	M + H	[61]
93	17.71	Syringetin	$C_{17}H_{14}O_8$	347.0754	347.0762	M + H	[70]
94	17.75	Tricin	$C_{17}H_{14}O_7$	331.0803	331.0813	M + H	[74]
95	18.05	Amentoflavone	$C_{30}H_{18}O_{10}$	537.0827	537.0827	M-H	[36]
96	18.34	Chrysoeriol	$C_{16}H_{12}O_6$	301.0698	301.0707	M + H	[71]
97	18.77	Ginkgetin 7-o-beta-d-glucopyranoside	$C_{38}H_{32}O_{15}$	727.1684	727.1668	M-H, M + FA-H	[78]
98	18.93	Isoginkgetin_7-o-beta-d-glucopyranoside	$C_{38}H_{32}O_{15}$	729.1795	729.1814	M + H	[78]
99	18.93	3-[5,7-dihydroxy_2-(4-methoxy-phenyl)-4-oxo-4 h-chromen_8-yl]-4-methoxy benzoic acid	$C_{24}H_{18}O_8$	435.1065	435.1075	M + H	
100	19.02	Hexadecanoic acid	$C_{16}H_{32}O_2$	301.2385	301.2385	M + FA-H	[79]
101	19.04	5,-methoxybilobetin	$C_{32}H_{22}O_{11}$	583.1221	583.1235	M + H	
102	19.08	Parthenolide	$C_{15}H_{20}O_3$	249.1478	249.1485	M + H	[80]
103	19.15	Chrysin	$C_{15}H_{10}O_4$	255.0644	255.0652	M + H	[81]
104	19.24	Roburic acid	$C_{30}H_{48}O_2$	441.3715	441.3727	M + H-H_2O, M + H	[82]
105	19.36	Genkwanin	$C_{16}H_{12}O_5$	283.0612	283.0612	M-H	[36]
106	19.37	Casticin	$C_{19}H_{18}O_8$	375.1065	375.1075	M + H	[83]
107	19.37	Acacetin	$C_{16}H_{12}O_5$	285.0748	285.0758	M + H	[84]
108	19.41	Galangin	$C_{15}H_{10}O_5$	269.0455	269.0455	M-H	[85]
109	19.45	Bilobetin	$C_{31}H_{20}O_{10}$	551.0988	551.0984	M-H	[36]
110	19.47	Kaempferide	$C_{16}H_{12}O_6$	301.0697	301.0707	M + H	[86]
111	19.52	Nobiletin	$C_{21}H_{22}O_8$	403.1378	403.1388	M + H	[81]
112	19.67	Pectolinarigenin	$C_{17}H_{14}O_6$	315.0853	315.0863	M + H	[75]
113	20.44	Isoginkgetin	$C_{32}H_{22}O_{10}$	567.1270	567.1286	M + H, 2 M + H	[36]

Table 1. *Cont.*

No.	tR/ (min)	Name	Formula	*m/z*	Expected *m/z*	Adducts	Reference
114	21.89	Ruvoside deglycosylation	$C_{23}H_{34}O_5$	389.2336	389.2333	M-H	[36]
115	22.05	Sciadopitysin	$C_{33}H_{24}O_{10}$	581.1429	581.1443	M + H, 2 M + H	[36]
116	22.69	6-tridecylresorcylic acid	$C_{20}H_{32}O_4$	319.2258	319.2268	M + H-H_2O, M + H	[87]
117	22.90	Hydroginkgolinic acid	$C_{21}H_{34}O_3$	333.2437	333.2435	M-H	[87]
118	23.92	Bilobol	$C_{21}H_{34}O_2$	317.2485	317.2486	M-H	[88]
119	24.08	Scillaren a deglycosylation	$C_{24}H_{32}O_4$	385.2363	385.2374	M + H	[48]
120	25.18	Anacardic acid d	$C_{22}H_{30}O_3$	341.2121	341.2122	M-H	[87]
120	25.85	Anacardic acid c	$C_{22}H_{32}O_3$	343.2277	343.2278	M-H	[89]
122	26.42	6-tridecylsalicylic acid	$C_{20}H_{32}O_3$	319.2277	319.2278	M-H	[90]
123	26.46	6-[(8z)-pentadecenyl]-salicylic acid	$C_{22}H_{34}O_3$	347.2577	347.2581	M + H-H_2O, M + H	[86]

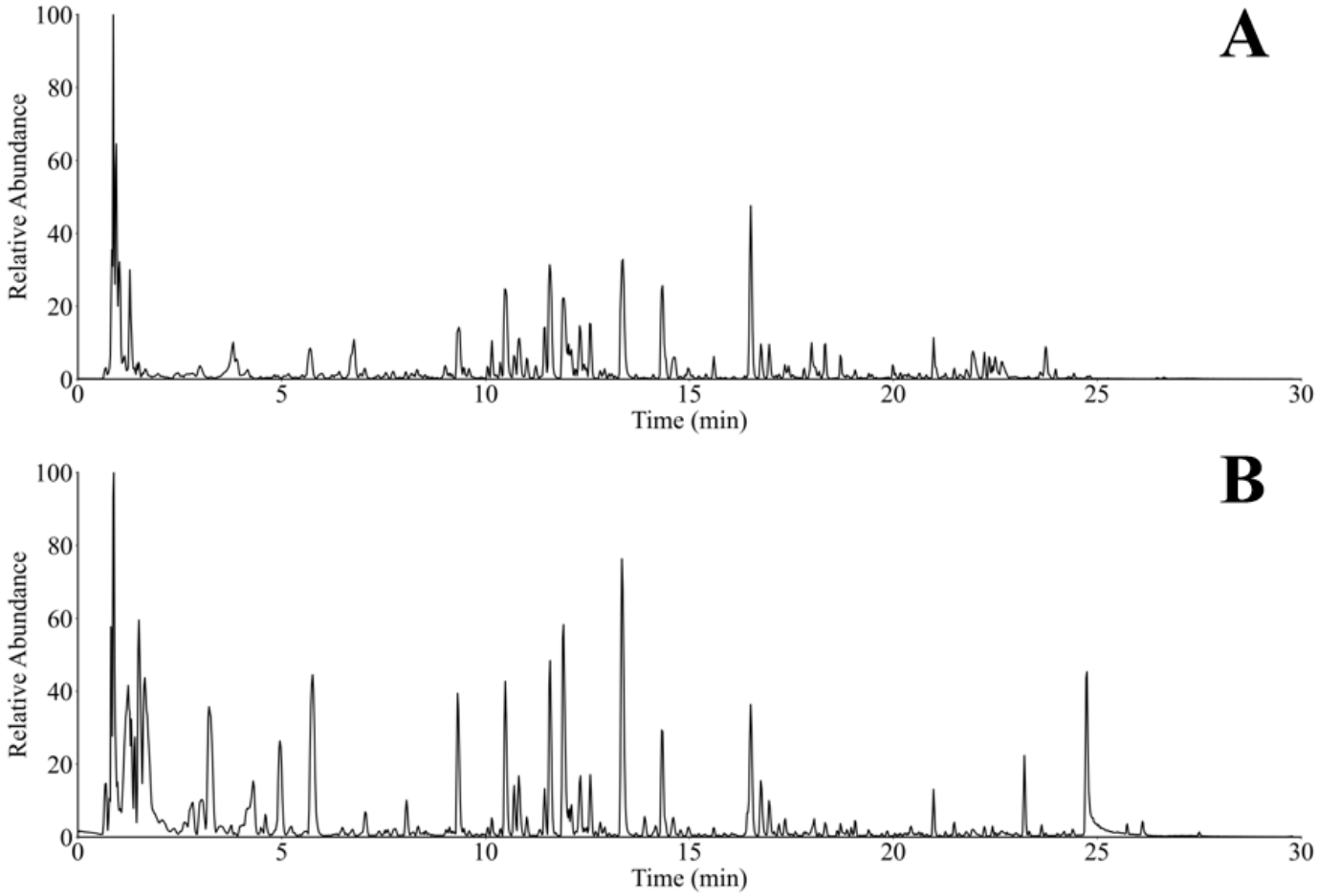


Figure 1. BPI of GBF detected in negative (**A**) and positive (**B**) mode.

2.2. GBF Promotes Skin Wound Healing in Normal Rats

To validate whether GBF promotes the healing of normal skin wounds, experiments were conducted in vivo to observe wound area changes over a 14-day period. The wound healing rate increased progressively across all groups over time (Figure 2A,B). On day 4, the recovered wound area rate in the GBF group was extremely significantly higher than that in the control group ($p < 0.0001$), and this superiority persisted until the end of the

experiment ($p < 0.01$). Notably, GBF outperformed the NJ (medical biological gel) group, and wounds were nearly fully healed by the 14th day with a 95% healing rate.

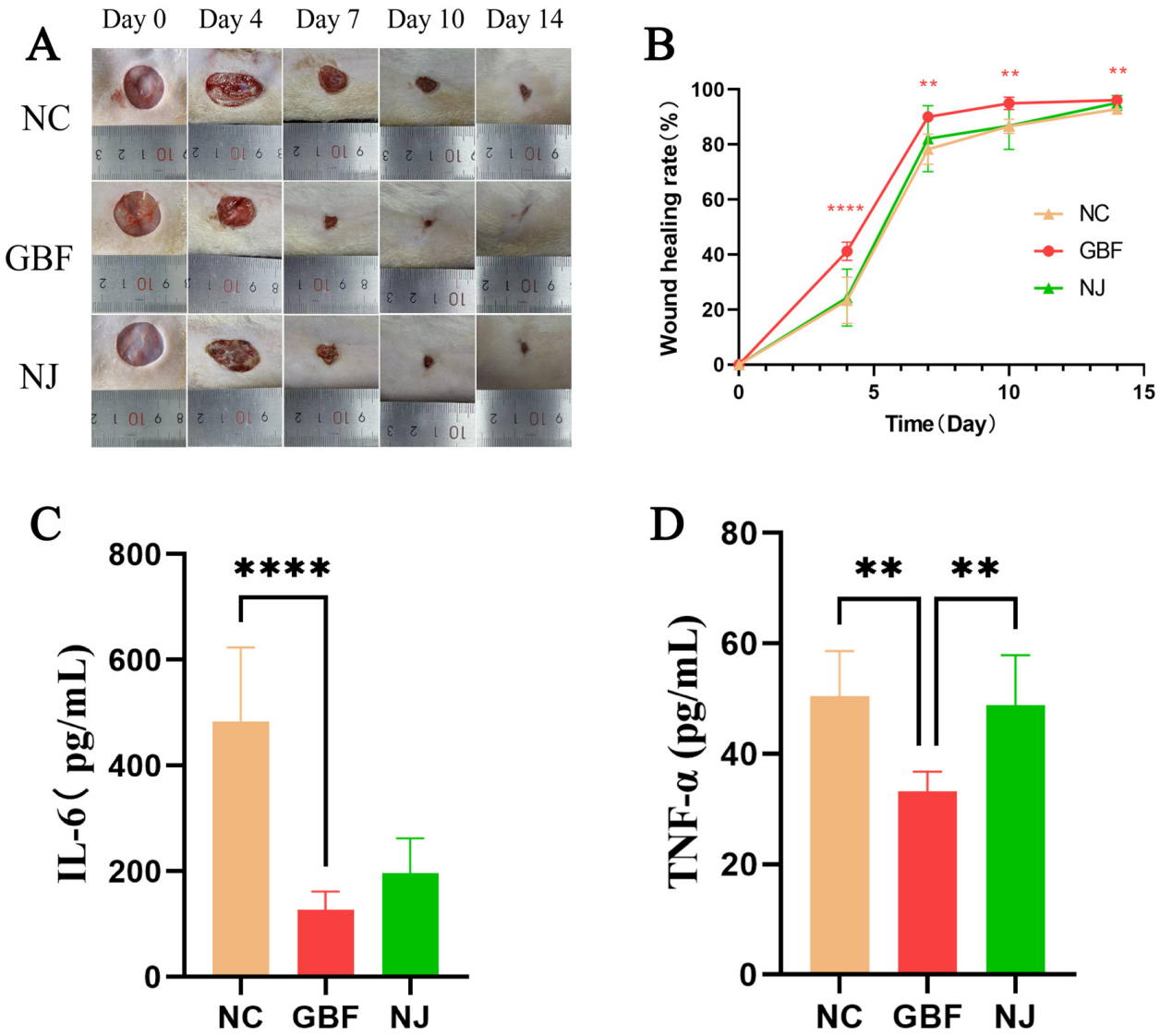


Figure 2. GBF promotes common wound healing in vivo. (**A**) Representative images of wound changes in rats in each group over 14 days. (**B**) Wound healing rate statistics. (**C**,**D**) Content of IL-6 and TNF-α in wound tissue samples on day 14. The results are shown as the mean ± standard deviation (SD), with a sample size of $n = 11$. Statistical significance was determined with the following levels: ** $p < 0.01$, and **** $p < 0.0001$.

Then, the inflammatory cytokines TNF-α and IL-6 in wound tissues were quantified. Compared with the control group (Figure 2C), the GBF group exhibited a dramatic reduction in IL-6 levels ($p < 0.0001$), which is additionally lower than the NJ group. Consistent with IL-6 (Figure 2D), the TNF-α content of the GBF group showed a significant decrease ($p < 0.01$). These findings suggest that GBF exerts potent in vivo anti-inflammatory activity, consistent with our prior research in vitro [31].

2.3. GBF Accelerates Skin Wound Healing in Diabetic Rats

Following confirmation of GBF's normal wound-repairing efficacy, its therapeutic potential for diabetic wounds was further evaluated. The experimental procedure is shown in Figure 3. As shown in Figure 4A,B, the wound closure area increased gradually in all

diabetic rat groups over time. Compared to the DM group, GBF significantly increased the wound healing rate on days 4 ($p < 0.01$), 7 ($p < 0.01$), 10 ($p < 0.01$), and 14 ($p < 0.01$) post-modeling, with the efficacy superior to the positive control drug.

The H&E staining of wound tissues on day 14 (Figure 4C) revealed that wounds in the DM group remained unhealed, characterized by thin epithelial tissue, localized necrotic debris, prominent inflammatory cell infiltration, and loosely arranged dermal tissue. In contrast, the GBF group displayed thicker, fully re-epithelialized wounds, less inflammatory infiltration, denser dermal collagen alignment, and scattered skin appendages. Masson staining of the same regions to assess collagen deposition and remodeling showed that GBF promoted more robust collagen accumulation and fiber rearrangement than that of the DM group (Figure 4D).

Immunohistochemistry (IHC) and immunofluorescence (IF) were used to detect CD31 and VEGF in wound tissues. The IHC results indicated that GBF significantly up-regulated CD31 ($p < 0.001$) and VEGF ($p < 0.01$) expression relative to the DM group (Figure 4E–G). The IF analyses confirmed these findings, with GBF enhancing CD31 ($p < 0.01$) and VEGF ($p < 0.0001$) levels more effectively than the positive drug (Figure 4H–J). Collectively, these data indicated that GBF can facilitate neovascularization in wound tissues.

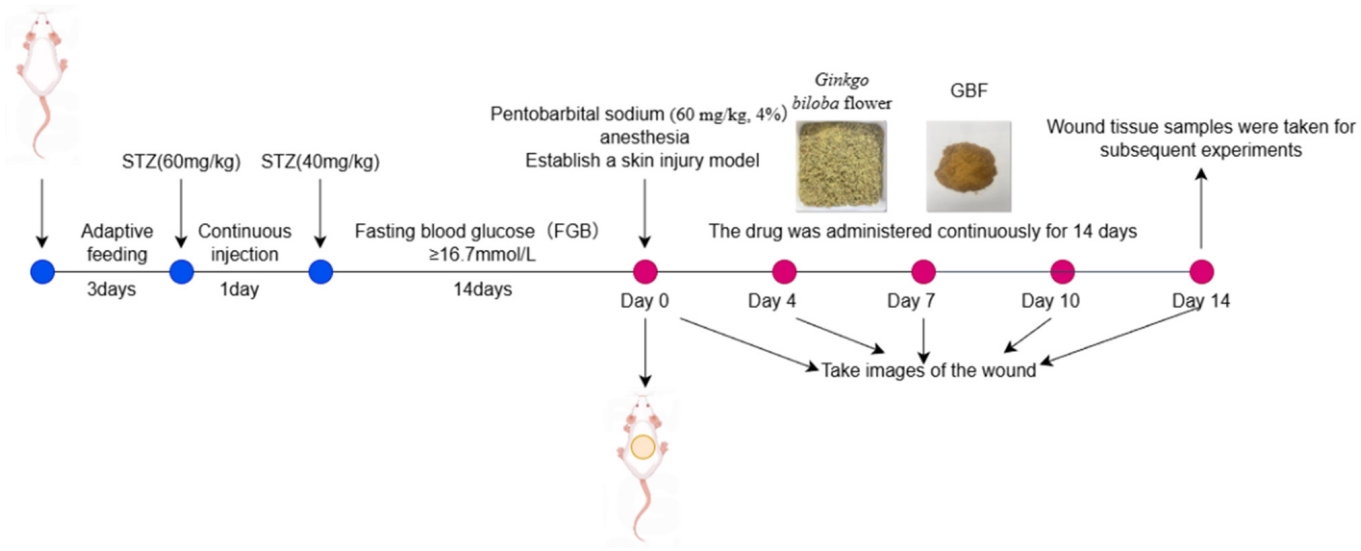


Figure 3. Schematic diagram of the establishment and administration of the skin injury model in diabetic rats.

2.4. GBF Suppresses Inflammation, Oxidative Stress and Ferroptosis in Diabetic Wounds

The inflammatory cytokines TNF-α and IL-6 in diabetic rat wound samples were then measured again. The GBF group showed markedly lower TNF-α ($p < 0.001$) and IL-6 ($p < 0.0001$) levels than the DM group (Figure 5A,B). Additionally, the oxidative stress marker GSH was significantly elevated by GBF compared to the DM group ($p < 0.0001$, Figure 5C). Western blotting was then employed to assess the expression of the ferroptosis marker GPX4 in wound tissues on day 14. The results showed that GBF significantly increased the GPX4 protein levels relative to the DM group ($p < 0.05$) (Figure 5D,E).

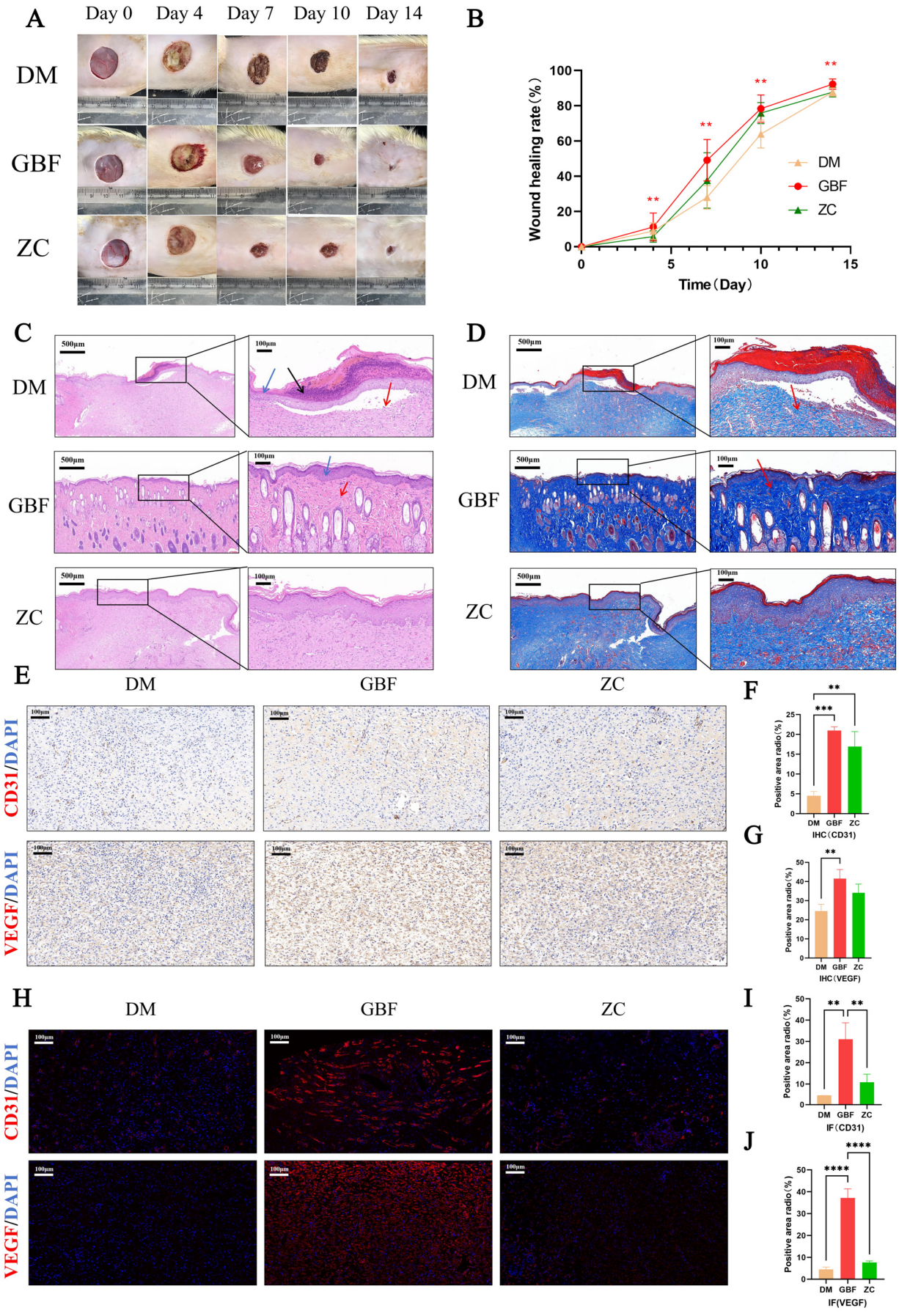


Figure 4. GBF promotes diabetic wound healing in vivo. (**A**) Representative images of wound changes in rats in each group over 14 days. (**B**) Wound healing rate statistics. (**C**) H&E staining was

used to evaluate the wound healing status of rats in each group. Epithelial tissue thickness (blue arrow), local necrotic tissue infiltrated by inflammatory cells (black arrow), dermal tissue arrangement (red arrow). Scale bar: 500, 100 μm. (**D**) Masson's trichrome staining was used to evaluate the wound healing status of rats in each group. Deposition and rearrangement of collagen fibers (red arrows). Scale bar: 500, 100 μm. (**E**–**G**) Immunohistochemistry was used to detect the expression of CD31 and VEGF in rat wound tissue. Scale bar: 100 μm. (**H**–**J**) Immunofluorescence was used to detect the expression of CD31 and VEGF in rat wound tissue. Scale bar: 100 μm. The results are shown as the mean ± standard deviation (SD), with a sample size of $n = 11$. Statistical significance was determined with the following levels: ** $p < 0.01$, *** $p < 0.001$, and **** $p < 0.0001$.

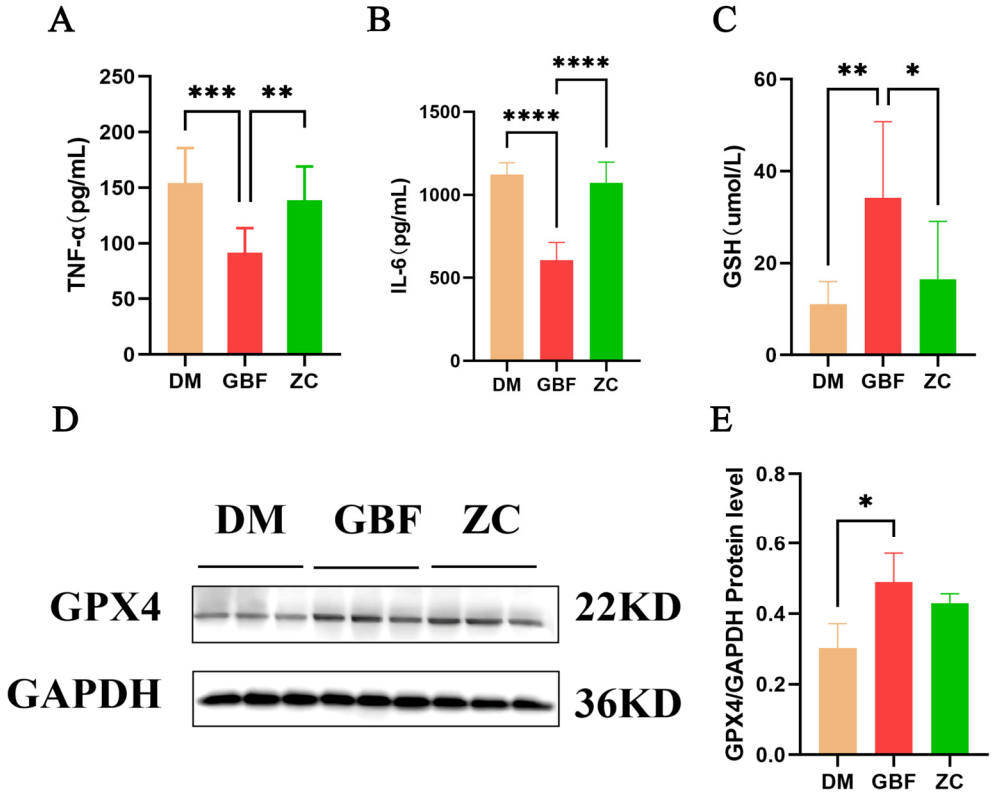


Figure 5. GBF can inhibit inflammation and ferroptosis in diabetic wounds. (**A**–**C**) The content of TNF-α,IL-6 and GSH was quantified using a commercial kit. $n = 8$. (**D**,**E**) The expression level of GPX4 was detected by Western blot. $n = 3$. The results are shown as the mean ± standard deviation (SD). Statistical significance was determined with the following levels: * $p < 0.05$, ** $p < 0.01$, *** $p < 0.001$, and **** $p < 0.0001$.

2.5. Proteomic Analysis in Diabetic Wounds

To elucidate the underlying mechanism of GBF in diabetic wound repair, label-free quantitative proteomic analysis was performed on rat skin wound tissue after 14 days of percutaneous wound modeling. Among the 6627 consistently quantified proteins, principal component analysis (PCA) showed significant separation between groups (Figure 6A–C). Based on the criteria of fold change (FC) > 1.5 or < 1/1.5 with a $p < 0.05$, we identified 1578 significantly altered proteins (712 up-regulated and 866 down-regulated) between the NC and DM groups (Figure 6D). Hierarchical clustering analysis revealed that these proteins had unique expression patterns, with color intensity indicating relative abundance (Figure 6E), confirming a significantly altered proteomic profile in the wound tissue of diabetic rats.

Candidate proteins were selected based on two significantly differentially expressed proteins (FC > 1.5 or < 1/1.5, $p < 0.05$) that were associated with ferroptosis and inflammation. Subsequently, PRM validated 27 candidate genes. The results showed that 16 proteins

(6 up-regulated and 10 down-regulated) were significantly altered in the DM group. GBF treatment reversed the changes in the above key proteins (Figure 6F–H). These PRM-validated target proteins may be potential regulatory mediators of GBF's anti-inflammatory and anti-ferroptosis effects in diabetic wounds.

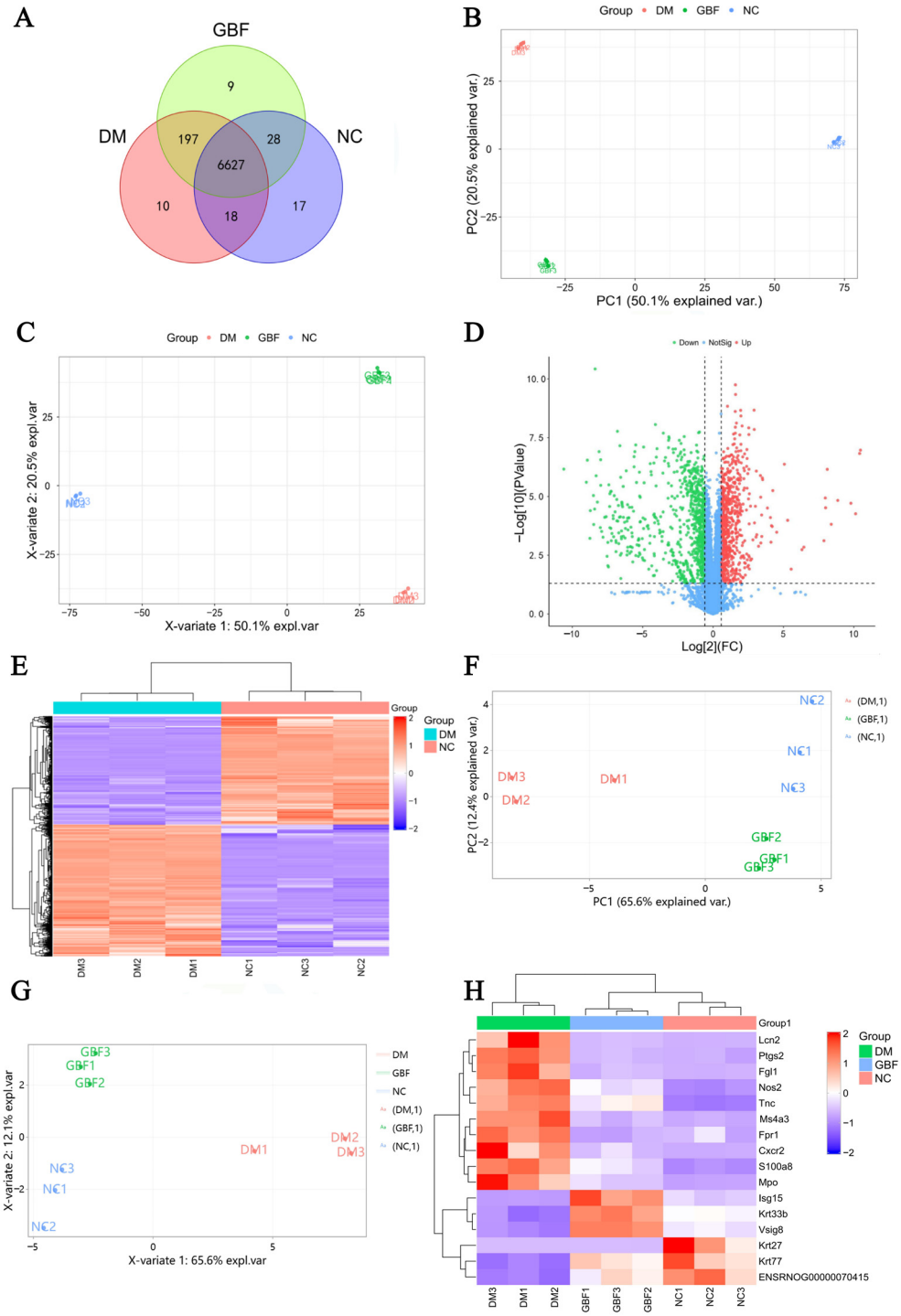


Figure 6. *Cont.*

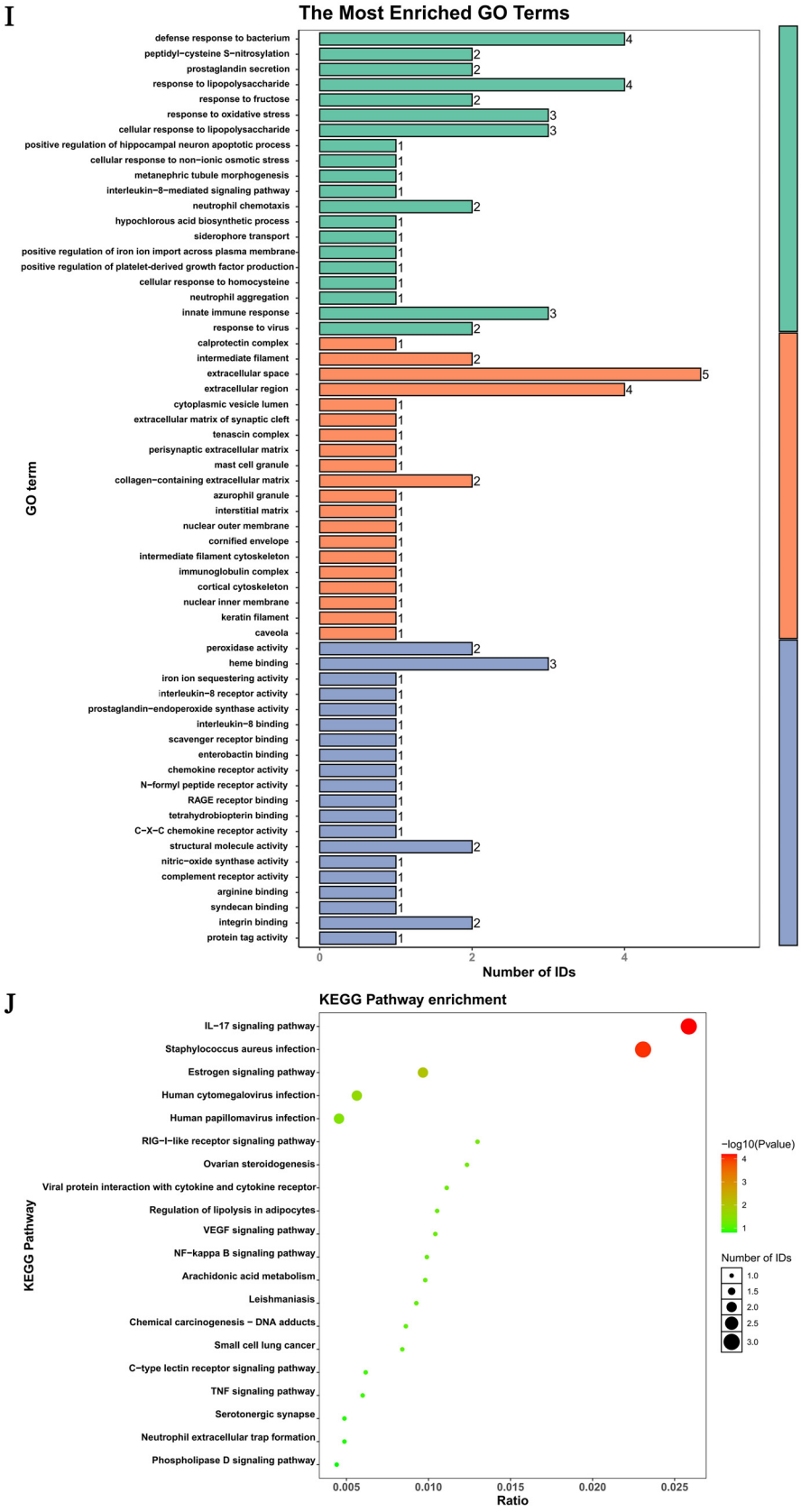


Figure 6. Proteomic analysis revealed the regulation of protein expression in GBF diabetic wounds. (**A**) Venn diagram of proteins between sample groups. (**B**) Plot of principal component analysis (PCA) scores. (**C**) Partial least squares discriminant analysis (PLS-DA) score plot. (**D**) Volcano plot of differentially expressed proteins. Red dots: up-regulated proteins; green dots: down-regulated proteins. (**E**) Heat map of 1578 differentially expressed proteins between NC group and DM group

identified by label-free untargeted proteomics. Blue and red indicate down-regulation and up-regulation, respectively. (**F**,**G**) PCA and PLS-DA score map of targeted proteomics analysis. (**H**) Heat map of differentially expressed proteins in NC group, DM group and GBF group shown by targeted proteomics analysis based on proteome relative enrichment matrix (PRM). (**I**) GO enrichment analysis (comparison between DM group and GBF group). (**J**) KEGG pathway enrichment analysis (comparison between the DM group and the GBF group). Pathways were ranked by enrichment ratio. Dot size reflects the amount of protein.

To further characterize the functional annotations of the identified proteins, Gene Ontology (GO) enrichment analysis was performed across three ontological categories: biological process (BP), cellular component (CC), and molecular function (MF) (Figure 6I). The differentially expressed proteins were significantly enriched in a wide range of GO terms, revealing critical insights into the underlying biological mechanisms. Significantly enriched in BP terms associated with inflammatory response were "response to lipopolysaccharide", "cellular response to lipopolysaccharide" "neutrophil chemotaxis", and "peptidyl-cysteine S-nitrosylation". In addition, "response to oxidative stress" was also significantly enriched. It is worth noting that "Multiple terms related to iron metabolism and transport such as" siderophore transport " and" positive regulation of iron ion import across plasma. "Membrane" was also significantly enriched, suggesting a potential association of ferroptosis in GBF repair of diabetic wounds. In CC classification, enriched terms mainly reflected extracellular matrix and structural protein features, such as "extracellular space", "extracellular region", "collagen-containing ECM", "intermediate filament", and "cornified envelope"; these results show the remodeling of the extracellular microenvironment and significant changes in the cytoskeleton structure. To demonstrate the relevance of GBF in diabetic skin wound healing or barrier function reconstruction, the MF category revealed enrichment in "heme binding", "peroxidase activity", "IL-8 receptor activity ", "chemokine receptor activity", and "RAGE receptor binding". These responses are associated with oxidative stress and inflammation. Collectively, the GO enrichment analysis demonstrates that the differentially expressed proteins are predominantly involved in inflammatory and immune responses, oxidative stress regulation, iron homeostasis, and extracellular matrix remodeling.

KEGG pathway enrichment analysis of the proteomic data revealed that GBF may regulate multiple biological processes (Figure 6J). The significantly enriched pathways covered multiple functional domains. Notably, the IL-17 signaling pathway, TNF signaling pathway, and NF-kappa B signaling pathway were identified, suggesting a potential involvement of inflammatory and immune regulatory mechanisms. Additionally, the VEGF signaling pathway was enriched, indicating a possible role in angiogenesis and vascular permeability regulation. Other enriched pathways, such as arachidonic acid metabolism, neutrophil extracellular trap formation, and the phospholipase D signaling pathway, further support the involvement of lipid metabolism and innate immune responses. These enrichment results showed that the differentially expressed proteins were mainly involved in inflammatory signal transduction, immune response and metabolic regulation. The multi-pathway regulation mechanism of GBF provides an important basis for its molecular mechanism of action in diabetic wound repair.

2.6. GBF Inhibits Ferroptosis and Enhances Viability in Rat Skin Fibroblasts (RS1)

CCK-8 assays were used to evaluate GBF's cytotoxicity on RS1 cells. Figure 7A shows that the 50–400 μg/mL GBF promoted RS1 proliferation in a dose-dependent manner. At a concentration of 400 μg/mL, RS1 cell viability was enhanced to approximately 110% relative to the negative control ($p < 0.001$), while the GBF of 800 μg/mL significantly suppressed cell viability ($p < 0.001$). The RS1 cells were then treated with varying concentrations of the

ferroptosis inducer erastin. As displayed in Figure 7B, the 5–20 μmol/L erastin remarkably reduced RS1 survival ($p < 0.0001$), and the 10 μmol/L erastin decreased cell viability to nearly 50% ($p < 0.0001$). Thus, the 10 μmol/L erastin was selected to establish an RS1 ferroptosis model for investigating GBF's inhibitory effects. The 50–400 μg/mL GBF treatment exhibited a dose-dependent rescue of erastin-induced RS1 cells ($p < 0.0001$). At the dose of 400 μg/mL, GBF increased the cell viability to 81% (Figure 7C). Fluorescence microscopy revealed that erastin induction significantly elevated intracellular Fe^{2+} levels ($p < 0.0001$), while 400 μg/mL GBF dramatically reduced Fe^{2+} concentrations ($p < 0.0001$)—with efficacy superior to the positive drug Ferrostatin-1 (Fer-1) (Figure 7D,E). Flow cytometry analysis of reactive oxygen species (ROS) showed that erastin markedly increased the ROS levels in RS1 cells ($p < 0.0001$), whereas GBF significantly attenuated ROS accumulation ($p < 0.0001$) more effectively than Fer-1 (Figure 7F,G), indicating GBF can mitigate oxidative stress in ferroptosis cells. Furthermore, the scratch assays demonstrated that erastin drastically impaired the migration rate of RS1 ($p < 0.0001$) after treatment for 24 h, while GBF significantly restored the migration capacity ($p < 0.001$) with a better efficacy than Fer-1 (Figure 7H,I).

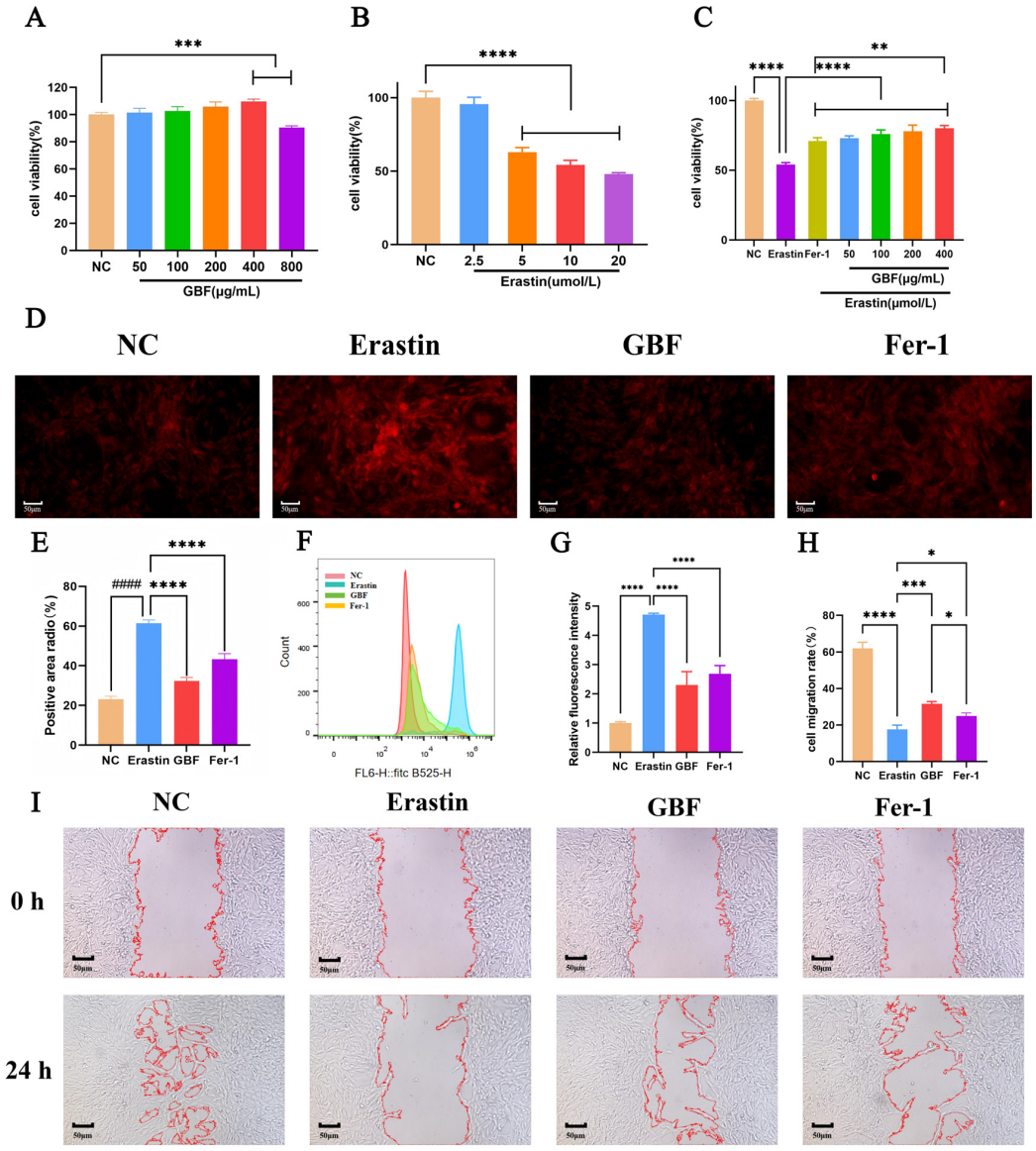


Figure 7. GBF can improve RS1's activity by inhibiting ferroptosis. (**A**) CCK-8 assays evaluated GBF's cytotoxicity on RS1 cells. (**B**) CCK-8 assay was used to detect the ferroptosis activity of RS1 cells induced by different concentrations of erastin. (**C**) CCK-8 assay was used to detect the activity of

GBF and Fer-1 on ferroptosis cell RS1. (**D**,**E**) The expression intensity of Fe^{2+} in cells was detected by immunofluorescence. Scale bar: 50 μm. (**F**,**G**) The expression of ROS was detected by flow cytometry. (**H**,**I**) Images and data statistics of cell migration area at 24 h in each group. Scale bar: 50 μm. The results are shown as the mean ± standard deviation (SD), with a sample size of $n = 3$. Statistical significance was determined with the following levels: * $p < 0.05$, ** $p < 0.01$, *** $p < 0.001$, **** $p < 0.0001$ and #### $p < 0.0001$.

3. Materials and Methods

3.1. Materials

Fresh male inflorescences of *Ginkgo biloba* L., the sole surviving species of the class Ginkgoopsida within the division Gymnospermae, were manually harvested in April 2023 from Tancheng County, Shandong Province, China. The botanical identity was authenticated by Professor Li of our laboratory. The voucher specimen (Accession No. GBF230415) is deposited in Beijing Academy of Military Medical Sciences.

Medical bio-gels (NJ), mainly composed of sodium alginate and carboxymethyl chitosan, are widely used as wound dressings to accelerate wound healing [91]. Wang et al. found that Zhu Zi ointment (Zi Cao ointment) promoted macrophage polarization by activating the PI3K/AKT pathway, thereby inhibiting inflammation and promoting ulcer wound healing [92]. Therefore, this study selected medical bio-gel as the common wound in vivo and Zi Cao (ZC) ointment as the positive drug for the diabetic wound study.

3.2. Determination of Chemical Composition

3.2.1. Sample Preparation

A 50mg sample of GBF and 1 mL of 80% methanol were loaded into a 1.5 mL centrifuge tube and sonicated for 30 min. Then, 0.2 mL of the suspension and 0.2 mL of 80% methanol were transferred to a 1.5 mL tube and centrifuged at 12,000 rpm for 10 min at 4 °C. Finally, 100 μL of the supernatant was injected for testing.

3.2.2. Chromatographic Method

A Vanquish Flex UHPLC chromatograph (Thermo Fisher Scientific, Inc., Waltham, MA, USA) equipped with an ACQUITY UPLC HSS T3 column was used for separation. The mobile phase consisted of water (0.1% formic acid, phase A) and acetonitrile (phase B) at a flow rate of 0.3 mL/min. The column temperature was 40 °C. The mobile-phase gradients were the following: 0–1 min: 2%B; 1–14 min: 2–30% B; 14–25 min: 30–100% B; 25–28 min: 100% B.

3.2.3. Mass Spectrometry Method

The MS data were collected by a hybrid quadrupole orbitrap mass spectrometer (Q Exactive, Thermo Fisher Scientific, Inc., Waltham, MA, USA) equipped with a HESI-II spray probe. The parameters were set as follows: the ion source voltages of positive (ESI+) and negative (ESI-) ions were 3.7 kV and 3.5 kV, respectively. The capillary heating temperature was 320 °C. The sheath gas pressure was 30 psi and the auxiliary gas pressure was 10 psi. The solvent heating evaporation temperature was 300 °C; the sheath gas and auxiliary gas were nitrogen. The collision gas was nitrogen at a pressure of 1.5 mTorr. The mass-to-charge ratio scanning range was from 100 to 1500.

3.3. Preparation of Extract

The collected air-dried male inflorescences of *Ginkgo biloba* L were cleaned to remove impurities. Subsequently, 200 g of the material was immersed in 70% aqueous ethanol. After 48 h of maceration, reflux extraction was performed for four cycles, each lasting 2 h. The combined extracts were concentrated under reduced pressure to remove the

solvent, yielding a crude extract. The extract was dispersed in a suitable volume of water and then successively extracted with petroleum ether. The extraction was repeated until the petroleum ether layer became colorless. The combined petroleum ether phases were concentrated using a rotary evaporator (BUCHI, Flawil, Switzerland) and then dried under vacuum to obtain the GBF [29,31].

3.4. Animals Experiment

Male Sprague Dawley (SD) rats were purchased from Beijing Sibef Biotechnology (Beijing, China) Co., Ltd. The rats were specific-pathogen-free (SPF), aged 6–8 weeks, and weighed 190–210 g. They were housed in a controlled-environment room maintained at 24–26 °C and 40–60% relative humidity, with a 12 h/12 h light–dark cycle. Food and water were available ad libitum. The Experimental Animal Ethics Committee of the Beijing Academy of Military Medical Sciences approved the animal experiments.

3.5. Establishment of Skin Injury Model in Normal Rats

The rats were anesthetized by intraperitoneal administration of sodium pentobarbital (60 mg/kg, 4% solution, Beijing, China). The dorsal hair was shaved, and any remaining hair follicles were thoroughly removed using a depilatory cream (Veet, Jingzhou, Hubei, China). Following disinfection with iodophor, a circular full-thickness skin open wound (20 mm in diameter) was marked on the shaved dorsal skin adjacent to the spine using a biopsy punch (Cellvis, Hangzhou, China).

For the wound healing assay, rats were randomly assigned to three groups (n = 11): the negative control (NC) group, medical biological gel (NJ) (Zhende Medical, Laoshan,, China) group, and the GBF group. The GBF solution of 20 mg/mL was applied topically to the wounds of each rat in the GBF group by means of spray daily. The NJ and NC groups received an equivalent volume of biological gel applied to cover the wound or normal saline (sprayed), respectively. The wound areas were photographed on days 0, 4, 7, 10, and 14 following the induction of the wounds. The captured images were analyzed using ImageJ software V1.4.4 to quantify the wound area. The wound healing rate was calculated as follows: [(initial wound area—unhealed area)/initial wound area] × 100%. At 14 days, the rats were euthanized, after which the wound tissues were collected for further experiments.

3.6. Establishment of Skin Injury Model in Diabetic Rats

Diabetes was induced by two intraperitoneal injections of streptozotocin (STZ, Solarbio, Beijing, China). The first injection was administered at a dose of 60 mg/kg, followed 24 h later by a second injection at 40 mg/kg. Two weeks later, fasting blood glucose (FBG) levels were measured daily for three consecutive days using a glucometer (Yuwell, Danyang, China), with blood samples obtained from the tail vein. Rats with FBG levels $\geq$ 16.7 mmol/L on all three days were considered diabetic, indicating successful model establishment.

The diabetic skin wound model was established following the procedure described for the normal wound model (Section 2.4). Rats were randomly divided into three groups (n = 8): the negative control (NC) group, the Zi Cao ointment (ZC) (Catalong Pharmaceutical, Kunming, China) group, and the GBF group. Treatments were administered, and wound healing rates were assessed as outlined in the normal wound experiment (Section 2.5).

3.7. Hematoxylin and Eosin (H&E) Staining

Following the collection of wound skin samples, they were fixed in 4% paraformaldehyde solution (Solarbio, Beijing, China). Subsequently, the samples underwent dehydration

using absolute ethanol, were embedded in paraffin, and sectioned into 5 μm thick sections. After H&E (Servicebio, Wuhan, China) staining, the tissue sections were examined under a light microscope (Olympus, Nagano, Japan), and representative images were captured.

3.8. Masson's Trichrome Staining

Wound skin samples were fixed in 4% paraformaldehyde solution (Solarbio, Beijing, China). Subsequently, the samples underwent dehydration using absolute ethanol, were embedded in paraffin, and sectioned into 5 μm thick sections. The sections were then subjected to Masson's trichrome (Servicebio, Wuhan, China) staining. Finally, the stained sections were examined and imaged using a light microscope (Olympus, Nagano, Japan).

3.9. Immunohistochemistry and Immunofluorescence

The 4% paraformaldehyde (Solarbio, Beijing, China) fixed tissue sections were subjected to dewaxing and dehydration procedures, followed by antigen retrieval and slide mounting. Endogenous peroxidase activity was then quenched, and non-specific binding sites were blocked with serum. The sections were subsequently incubated overnight at 4 °C with the following primary antibodies: rabbit anti-CD31 antibody (1:500, Servicebio, Wuhan, China) and rabbit anti-VEGF antibody (1:250, Servicebio, Wuhan, China). After washing with phosphate-buffered saline (PBS), the sections were incubated with HRP-conjugated goat anti-rabbit IgG secondary antibody (Servicebio, Wuhan, China) at room temperature for 50 min. Counterstaining was performed using hematoxylin, and sample images were acquired using a light microscope (Olympus, Nagano, Japan). Finally, the quantitative image analysis was conducted using Image J software V1.4.4.

The subsequent sample preparation and antigen retrieval steps remain unchanged as outlined in the Immunohistochemistry section. The sections were subsequently incubated overnight at 4 °C with the following primary antibodies: rabbit anti-CD31 antibody (1:100, Servicebio, Wuhan, China) and rabbit anti-VEGF antibody (1:200, Servicebio, Wuhan, China). After washing with phosphate-buffered saline (PBS), the sections were incubated with CY3-conjugated goat anti-rabbit IgG secondary antibody (Servicebio, Wuhan, China) at room temperature for 50 min. The nuclei were counterstained with DAPI (Servicebio, Wuhan, China), and tissue autofluorescence was quenched using an autofluorescence quenching agent (Servicebio, Wuhan, China). Finally, the sections were imaged under a fluorescence microscope (Nikon, Kanagawa, Japan) and the images were analyzed using ImageJ software V1.4.4.

3.10. Determination of GSH, TNF-α, IL-6, and GPX4

GSH levels in wound tissue samples were determined using a Total Glutathione/Oxidized Glutathione (T-GSH/GSSG) Assay Kit (Jiancheng Technology, Nanajing, China), strictly following the manufacturer's instructions.

TNF-α and IL-6 levels in wound tissue samples were determined using a Rat TNF-α Precoated ELISA Kit (Dayou Biology, Shenzhen, China) and Rat IL-6 Precoated ELISA Kit (Dayou Biology, Shenzhen, China), strictly following the manufacturer's instructions.

The tissues were homogenized in RIPA lysis buffer (Applygen, Beijing, China) to extract the total protein. Protein concentrations were determined using a BCA assay (Applygen, Beijing, China) to ensure equal loading across all wells. The proteins were then separated by electrophoresis on 12.5% SDS–polyacrylamide gels (Applygen, Beijing, China) and transferred onto polyvinylidene difluoride (PVDF) membranes (Merck, Shanghai, China). After blocking, the membranes were incubated overnight at 4 °C with the following primary antibodies: anti-GPX4 (1:1000, Abcam, Cambridge, UK) and anti-GAPDH (1:500, Servicebio, Wuhan, China). Subsequently, the membranes were incubated with horseradish peroxidase (HRP)-conjugated secondary antibodies (Abcam, Cambridge, UK) for 1 h at

room temperature. The protein bands were visualized using a chemiluminescence imaging system (Bio-Rad Laboratories, Hercules, CA, USA), and their relative intensities were quantified with ImageJ software V1.4.4.

3.11. Proteomics Analysis

Data-Independent Acquisition Proteomics was used to compare the differences in protein expression among the NC, DM and GBF groups. In addition, a parallel response monitoring (PRM) technique was used to verify the regulatory effect of GBF on the differential protein expression in the wounds of diabetic rats. Protein identification was performed by UPLC-MS/MS (Qinglian Biotechnology, Beijing, China). Data processing was done using ProteomeDiscoverer (v2.4) and Skyline software (v23.1).

3.12. Cell Culture

RS1 cells (Fuheng Biology, Shanghai, China) were cultured in DMEM medium (Macgene Biotechnology, Beijing, China) containing 1% streptomycin and penicillin (Macgene Biotechnology, Beijing, China), and 10% fetal bovine serum (FBS) (Gibco, Grand Island, NY, USA) in a cell incubator (Thermo Fisher Scientific, Waltham, MA, USA, 37 °C, 5% CO_2).

3.13. Cell Viability

The 5×10^3 cells were seeded into 96-well plates in a cell culture incubator for 8 h. Subsequently, GBF solutions at varying concentrations (0, 50, 100, 200, 400, 800 μg/mL) were added to evaluate the cytotoxicity of GBF. Under identical culture conditions, erastin (Selleck, Houston, TX, USA) at concentrations of 0, 2.5, 5, 10, and 20 μmol/L was administered to determine the optimal concentration for inducing ferroptosis. Finally, GBF solutions at different concentrations (50, 100, 200, 400 μg/mL) were added, with 1 μmol/L ferroptosis inhibitor Ferrostatin-1 (Fer-1, Selleck, Houston, TX, USA) serving as a positive control, to investigate the inhibitory effect of GBF on ferroptosis in RS1 cells. Twenty-four hours after treatment initiation, 10 μL of CCK-8 reagent (Meilun Biology, Dalian, China) was added to each well, followed by incubation in a 37 °C incubator for 40 min. Absorbance was measured at a wavelength of 450 nm using a microplate reader (Thermo Sciectific, Singapore) and cell viability was subsequently calculated and compared.

3.14. ROS and Fe^{2+} Determination

The DCFH-DA (Elabscience, Wuhan, China) was used to detect ROS levels. The experimental method was to inoculate 5×10^5 cells into 6-well plates and divide them into the following groups, NC (negative control), erastin (10 μmol/L), Fer-1 (1 μmol/L), and GBF (400 μg/mL), and they were then cultured in a cell incubator for 8 h. The cells were washed twice with PBS and then incubated with DCFH-DA at 37 °C for 30 min in the dark. Following a final wash, cells were collected and analyzed by flow cytometry to determine and compare intracellular ROS levels across groups.

The 575 Red Fe^{2+} Dye (BioTracker, St. Louis, MO, USA) was used to detect Fe^{2+} levels. The experimental method was to inoculate 5×10^5 cells into 6-well plates and divide them into the following groups, NC, erastin (10 μmol/L), Fer-1 (1 μmol/L) and GBF (400 μg/mL), and they were then cultured in a cell incubator for 8 h. The cells were washed twice with serum-free medium and then incubated with 575 Red Fe^{2+} Dye at 37 °C for 60 min in the dark. Following a final wash, cell fluorescence intensity was measured using fluorescence microscopy.

3.15. Scratch Assay

To investigate the effect of GBF on RS1 cell migration, a scratch assay was conducted on a confluent cell monolayer. The specific steps were to inoculate cells into 6-well plates

and divide them into the following groups: NC, erastin (10μmol/L), Fer-1 (1 μmol/L), and GBF (400 μg/mL). Once the cell density reached 95%, the cells were scratched using a 200 μL sterile plastic tip. Following this, the culture was sustained using a serum-free medium. The cell migration of each group was observed by a light microscope (Olympus, Nagano, Japan) after 24 h.

3.16. Statistical Analysis

The data were expressed as the mean value ± standard deviation. A one-way analysis of variance was conducted utilizing the GraphPad Prism, version 9.0.0 (GraphPad Software, San Diego, CA, USA), followed by the Dunnett multiple comparison test. All data were analyzed by pairwise comparison among multiple groups. Statistically speaking, p values are labeled as * $p < 0.05$, ** $p < 0.01$, *** $p < 0.001$, **** $p < 0.0001$.

4. Discussion

Diabetic wounds are one of the most serious complications of diabetes, with a large number of patients and a high disability and mortality rate. The adverse impact of diabetic ulcers not only seriously affects the quality of life of patients but also brings a heavy economic burden to society [93]. The process of wound healing mainly consists of four overlapping and distinct stages: hemostasis, inflammation, proliferation, and remodeling. These stages involve cell migration and proliferation, extracellular matrix deposition, and tissue remodeling [94]. Numerous studies have shown that various factors, such as persistent inflammation, impaired angiogenesis, oxidative stress, and slow cell growth in diabetic wounds, can have detrimental effects on wound healing [95–98]. Some research has also reported that ferroptosis inhibits wound healing in diabetic wounds [20,21,99].

Natural traditional Chinese medicine is widely used in the treatment of diabetic wounds. Total iridoid glycoside extract of L. rotata can accelerate diabetic wound healing through NRF2/COX2 axis [100]. Lonicerin facilitates angiogenesis and diabetic wound healing via Sirt1-mediated autophagy activation [101]. *Ginkgo biloba* L is a pharmacologically rich natural traditional Chinese medicine with documented antioxidant, anti-radiation, and cardioprotective properties [102]. Our previous studies have shown that GBF can inhibit ferroptosis in human umbilical vein endothelial cells by down-regulating ACSL4 expression and up-regulating GPX4 expression [31], and also inhibit ferroptosis in nerve cells by inhibiting ROS, LPO destruction and Fe^{2+} elevation [29]. GBF-8, a subcomponent isolated from GBF, reduced neuroinflammation and identified the Slc7a11-Eif4ebp1 axis as the main target of GBF-8 in inhibiting ferroptosis [103]. This is due to its potential active ingredient. The flavonoid ginkgetin can significantly reduce the expression of TNF-α, IL-6, IL-1β and other pro-inflammatory factors by inhibiting the TLR4/NF-κB signaling pathway, while up-regulating the anti-inflammatory factor IL-10 [104]. The flavonoid quercetin can inhibit ferroptosis of endothelial cells by regulating the KEAP1/NRF2/GPX4 signaling pathway [105]. Ginkgolide B, a terpene lactone, can alleviate oxidative stress and ferroptosis by inhibiting GPX4 ubiquitination [106]. We extended this investigation to examine its effects on diabetic wound healing, focusing on inflammation and ferroptosis regulation in vivo. TNF-α and IL-6 are pivotal pro-inflammatory cytokines. Their overexpression in wound tissue is a major barrier to healing [107,108]. In a normal rat wound model, GBF accelerated wound closure and reduced TNF-α/IL-6 levels, confirming its pro-healing and anti-inflammatory effects. GSH is a potent biological antioxidant that mitigates oxidative stress and plays an important role in the ferroptosis pathway [109,110]. The increase in the GSH content in the wound can promote wound healing [111]. In the diabetic rat model induced by multiple STZ injections, the wound tissue levels of TNF-α, IL-6, and GSH were measured. Compared with the DM group, GBF treatment significantly reduced the

levels of the pro-inflammatory cytokines TNF-α and IL-6, while increasing the content of the antioxidant GSH. These results suggest that GBF promotes diabetic wound healing by mitigating inflammation and alleviating oxidative stress. GPX4 plays a pivotal role in clearing excess lipid peroxides and is a central regulator of ferroptosis [112]. It mitigates ferroptosis induced by peroxide accumulation by catalyzing the GSH-dependent reduction of lipid hydroperoxides [113]. Western blot analysis demonstrated that GBF treatment up-regulated GPX4 expression compared to the DM group, confirming that GBF can inhibit ferroptosis in diabetic wounds.

VEGF is a key signaling molecule that specifically initiates angiogenesis, promoting the sprouting and growth of new blood vessels [114]. In contrast, CD31 is a transmembrane protein highly expressed at endothelial cell junctions. It serves as a marker of mature vascular endothelium, primarily involved in intercellular adhesion and the maintenance of vascular integrity and permeability, indicating the stabilization of nascent vessels into functional structures [115]. The concurrent up-regulation of both markers in wound tissue is a recognized hallmark of active and maturing angiogenesis. Our IHC and IF analyses of diabetic wound samples revealed that GBF treatment significantly increased the expression levels of both VEGF and CD31 compared to the DM group. This finding indicates that GBF effectively promotes neovascularization in diabetic wounds. Furthermore, histological assessment via H&E and Masson staining demonstrated that the GBF group exhibited superior wound coverage, along with enhanced collagen fiber deposition and remodeling relative to the DM group. Collectively, these results demonstrate that GBF facilitates diabetic wound healing by stimulating functional angiogenesis and improving the quality of tissue repair.

Proteomic analysis revealed that GBF modulates multiple pathways associated with inflammation, oxidative stress, ferroptosis, and angiogenesis in diabetic wounds. Label-free quantitative proteomics identified 1578 differentially expressed proteins between the NC and DM groups (FC > 1.5 or < 1/1.5, $p < 0.05$). Parallel reaction monitoring (PRM) validated 16 proteins (6 up-regulated, 10 down-regulated) in the DM group, whose abnormal expression was reversed by GBF treatment. GO enrichment analysis showed that the differentially expressed proteins were predominantly involved in inflammatory responses (response to lipopolysaccharide, neutrophil chemotaxis), oxidative stress, iron metabolism (siderophore transport, positive regulation of iron ion import), and extracellular matrix remodeling. KEGG pathway enrichment analysis identified key pathways including IL-17, TNF, NF-κB, and VEGF signaling, as well as arachidonic acid metabolism and neutrophil extracellular trap formation. Collectively, these proteomic findings indicate that GBF promotes diabetic wound healing through multi-pathway regulation of inflammation, oxidative stress, ferroptosis, and angiogenesis.

Dermal fibroblasts are pivotal functional cells in skin wound repair, driving healing through proliferation, redifferentiation, and the secretion of extracellular matrix components such as collagen and fibronectin across all four phases of wound healing. Insufficient fibroblast presence in wound skin is a key factor contributing to impaired healing in chronic conditions like diabetic wounds [116]. The occurrence of ferroptosis in fibroblasts is one of the factors affecting diabetic wound recovery [112]. In our experiments in vitro, various concentrations of GBF significantly restored the viability and migration rate of RS1 dermal fibroblasts that had been compromised by the ferroptosis inducer erastin. This indicates that GBF can promote fibroblast growth and function, thereby supporting its promoting effects on diabetic wound closure. Ferroptosis is characterized by Fe^{2+} overload and excessive generation of reactive ROS [14,117]. In erastin-induced ferroptotic RS1 cells, we further observed that GBF treatment effectively reduced both the Fe^{2+} and ROS levels.

Taken together, these findings suggest that GBF inhibits ferroptosis in dermal fibroblasts, which may in turn facilitate angiogenesis and enhance the healing of diabetic wounds.

Although GBF has been shown to regulate key ferroptosis-related proteins (GPX4) and inflammatory cytokines (TNF-α, IL-6), the upstream signaling pathways mediating these effects, such as the involvement of the Nrf2 and NF-κB signaling pathways, have not been systematically investigated. In the future, further studies using pathway-specific inhibitors or gene-silencing technology are needed to elucidate the precise molecular mechanism. Complex extract components may create potential confounding factors. GBF is a multicomponent extract containing 123 identified compounds, including flavonoids, terpenoids and other substances. Although this complexity may enhance their multi-target therapeutic utility, it also poses challenges for quality control, batch-to-batch consistency, and regulatory approval. We plan to establish a component separation platform to purify flavonoid and terpene lactone monomers individually, and to conduct comparative experiments to further verify their independent biological functions. Furthermore, based on the structural information of the chemical components, we intend to systematically delineate the structure–activity relationships of these compounds, clarify the impact of different core skeletons and functional groups on their pharmacological activities, and elucidate the synergistic mechanisms by which these components collectively improve diabetic wound healing.

5. Conclusions

This study demonstrates that GBF promotes diabetic wound healing through two aspects. On one hand, GBF inhibits key pathological processes—namely ferroptosis, inflammation, and oxidative stress. On the other hand, it enhances repair mechanisms by stimulating angiogenesis and tissue remodeling. Furthermore, GBF was found to promote the proliferation and migration of dermal fibroblasts, an effect closely associated with its inhibition of ferroptosis in these cells. Collectively, these findings identify GBF as a novel and promising natural product candidate for the development of therapeutics aimed at treating diabetic wounds.

Author Contributions: Conceptualization, X.S. and M.L.; methodology, X.S.; data curation, R.L., Y.W. and Y.X.; investigation, M.L. and S.L. (Shuchen Liu).; formal analysis, Z.X., Y.T., G.Z. and S.L. (Sifan Liu). writing—original draft preparation, X.S.; writing—review and editing, M.L. and S.L. (Shuchen Liu).; supervision, S.L. (Shuchen Liu).; All authors have read and agreed to the published version of the manuscript.

Funding: This research received no external funding.

Institutional Review Board Statement: All experimental procedures were approved by the Animal Care and Use Committee of the Academy of Military Medical Sciences and conducted in strict accordance with the institutional guidelines for the care and use of laboratory animals (Ethical approval No.DWZX-IACUC-2026-504).

Informed Consent Statement: Not applicable.

Data Availability Statement: The original data presented in this research are included in the article. Further inquiries can be directed to the corresponding authors.

Conflicts of Interest: The authors declare no conflicts of interest.

References

1. Wright, J.A.; Richards, T.; Srai, S.K.S. The Role of Iron in the Skin and Cutaneous Wound Healing. *Front. Pharmacol.* **2014**, *5*, 156. [CrossRef] [PubMed]

2. Lu, J.; Li, X.-Q.; Chen, P.-P.; Zhang, J.-X.; Li, L.; Wang, G.-H.; Liu, X.-Q.; Jiang, C.-M.; Ma, K.-L. Acetyl-CoA Synthetase 2 Promotes Diabetic Renal Tubular Injury in Mice by Rewiring Fatty Acid Metabolism through SIRT1/ChREBP Pathway. *Acta Pharmacol. Sin.* **2024**, *45*, 366–377. [CrossRef] [PubMed]
3. Balakumar, P. Unleashing the Pathological Role of Epithelial-to-Mesenchymal Transition in Diabetic Nephropathy: The Intricate Connection with Multifaceted Mechanism. *World J. Nephrol.* **2024**, *13*, 95410. [CrossRef] [PubMed]
4. Yang, T.-T.; Shao, Y.-T.; Cheng, Q.; He, Y.-T.; Qiu, Z.; Pan, D.-D.; Zhang, H.-M.; Jiang, Z.-Z.; Yan, M.; Ying, C.-J.; et al. YY1/HIF-1α/mROS Positive-Feedback Loop Exacerbates Glomerular Mesangial Cell Proliferation in Mouse Early Diabetic Kidney Disease. *Acta Pharmacol. Sin.* **2025**, *46*, 1974–1989. [CrossRef] [PubMed]
5. Liu, D.; Chen, X.; He, W.; Lu, M.; Li, Q.; Zhang, S.; Xie, J.; Zhang, Y.; Wang, W. Update on the Pathogenesis, Diagnosis, and Treatment of Diabetic Tubulopathy. *Integr. Med. Nephrol. Androl.* **2024**, *11*, e23. [CrossRef]
6. Julla, J.-B.; Jolivet, T.; Estellat, C.; Varoquaux, G.; Carlier, A.; Gautier, J.-F.; Alberge, J.; Abouleka, Y.; Bergès, A.; Liu, E.; et al. Incidence of Death and Amputation in Patients with a First Diabetic Foot Ulcer: Results from the CODIA Cohort. *Diabetes Metab.* **2025**, *51*, 101700. [CrossRef] [PubMed]
7. Wernecke, J.; Wernecke, M.; Ebenau, O.; Spruth, B.; Krämer, M.; Vogelmann, T.; Zöllner, Y. Epidemiology and the Medical Burden of Diabetic Foot Ulcers Especially in Patients with Infection—A Population-Based Analysis from Germany. *Int. Wound J.* **2025**, *22*, e70157. [CrossRef] [PubMed]
8. Feng, J.; Lai, S.; Tang, D. Mechanisms and Interventions of Diabetic Wound Healing. *Curr. Diabetes Rev.* **2026**, *22*, 147–160. [CrossRef] [PubMed]
9. Pavithra, T.R.; Kaliyaperumal, R. Epidemiology, Pathophysiology, and Management of Diabetic Foot: A Comprehensive Review. *Foot* **2026**, *66*, 102225. [CrossRef] [PubMed]
10. Lazzarini, P.A.; Armstrong, D.G.; Crews, R.T.; Gooday, C.; Jarl, G.; Kirketerp-Moller, K.; Viswanathan, V.; Bus, S.A. Effectiveness of Offloading Interventions for People with Diabetes-related Foot Ulcers: A Systematic Review and Meta-analysis. *Diabetes Metab. Res.* **2024**, *40*, e3650. [CrossRef] [PubMed]
11. Bardill, J.R.; Laughter, M.R.; Stager, M.; Liechty, K.W.; Krebs, M.D.; Zgheib, C. Topical Gel-Based Biomaterials for the Treatment of Diabetic Foot Ulcers. *Acta Biomater.* **2022**, *138*, 73–91. [CrossRef] [PubMed]
12. Mendoza-Marí, Y.; García-Ojalvo, A.; Fernández-Mayola, M.; Rodríguez-Rodríguez, N.; Martinez-Jimenez, I.; Berlanga-Acosta, J. Epidermal Growth Factor Effect on Lipopolysaccharide-Induced Inflammation in Fibroblasts Derived from Diabetic Foot Ulcer. *Scars Burn. Heal.* **2022**, *8*, 20595131211067380. [CrossRef] [PubMed]
13. Qi, X.; Cai, E.; Xiang, Y.; Zhang, C.; Ge, X.; Wang, J.; Lan, Y.; Xu, H.; Hu, R.; Shen, J. An Immunomodulatory Hydrogel by Hyperthermia-Assisted Self-Cascade Glucose Depletion and ROS Scavenging for Diabetic Foot Ulcer Wound Therapeutics. *Adv. Mater.* **2023**, *35*, 2306632. [CrossRef] [PubMed]
14. Yan, H.; Zou, T.; Tuo, Q.; Xu, S.; Li, H.; Belaidi, A.A.; Lei, P. Ferroptosis: Mechanisms and Links with Diseases. *Signal Transduct. Target. Ther.* **2021**, *6*, 49. [CrossRef] [PubMed]
15. McDermott, K.; Fang, M.; Boulton, A.J.M.; Selvin, E.; Hicks, C.W. Etiology, Epidemiology, and Disparities in the Burden of Diabetic Foot Ulcers. *Diabetes Care* **2023**, *46*, 209–221. [CrossRef] [PubMed]
16. Guan, Y.; Niu, H.; Liu, Z.; Dang, Y.; Shen, J.; Zayed, M.; Ma, L.; Guan, J. Sustained Oxygenation Accelerates Diabetic Wound Healing by Promoting Epithelialization and Angiogenesis and Decreasing Inflammation. *Sci. Adv.* **2021**, *7*, eabj0153. [CrossRef] [PubMed]
17. Liang, Z.; Gu, Y.; Li, Y.; Wu, Z.; Xu, X.; Wei, G.; Wang, N.; Zhang, Z.; Hao, Q.; Peng, Y.; et al. FGF21-Engineered ADSCs Promote Diabetic Wound Healing by Mitigating Ferroptosis and Oxidative Stress via the SIRT1/NRF2/GPX4 Signaling Pathway. *Stem Cell Res. Ther.* **2025**, *16*, 650. [CrossRef] [PubMed]
18. Huang, J.; Peng, Y.; Xiao, Y.; Wang, Y.; Hu, F. Loss of MAF bZIP Transcription Factor G Restores ATG7/BECN1-Mediated Autophagy to Inhibit Ferroptosis and Improve Angiogenesis in Diabetic Foot Ulcer Wound Healing. *Can. J. Diabetes* **2025**, *49*, 237–248.e1. [CrossRef] [PubMed]
19. Dai, W.; Shu, R.; Yang, F.; Li, B.; Johnson, H.M.; Yu, S.; Yang, H.; Chan, Y.K.; Yang, W.; Bai, D.; et al. Engineered Bio-Heterojunction Confers Extra- and Intracellular Bacterial Ferroptosis and Hunger-Triggered Cell Protection for Diabetic Wound Repair. *Adv. Mater.* **2024**, *36*, 2305277. [CrossRef] [PubMed]
20. Xiao, K.; Wang, S.; Li, G.; Chen, W.; Chen, B.; Li, X. Resveratrol Promotes Diabetic Wound Healing by Inhibiting Ferroptosis in Vascular Endothelial Cells. *Burns* **2024**, *50*, 107198. [CrossRef] [PubMed]
21. Lin, C.; Hu, Y.; Lin, Z.; Du, L.; Hu, Y.; Ouyang, L.; Xie, X.; Cheng, P.; Liao, J.; Lu, L.; et al. MMP-9 Responsive Hydrogel Promotes Diabetic Wound Healing by Suppressing Ferroptosis of Endothelial Cells. *Bioact. Mater.* **2025**, *43*, 240–254. [CrossRef] [PubMed]
22. Volpe, C.M.O.; Villar-Delfino, P.H.; dos Anjos, P.M.F.; Nogueira-Machado, J.A. Cellular Death, Reactive Oxygen Species (ROS) and Diabetic Complications. *Cell Death Dis.* **2018**, *9*, 119. [CrossRef] [PubMed]
23. Yin, J.; Xu, X.; Guo, Y.; Sun, C.; Yang, Y.; Liu, H.; Yu, P.; Wu, T.; Song, X. Repair and Regeneration: Ferroptosis in the Process of Remodeling and Fibrosis in Impaired Organs. *Cell Death Discov.* **2024**, *10*, 424. [CrossRef] [PubMed]

24. Liang, C.; Hao, P.; Gong, Z. Targeting Programmed Cell Death Pathways in Diabetic Foot Ulcers: Mechanisms and Therapeutic Strategies. *Int. J. Biochem. Cell Biol.* **2026**, *197–198*, 106947. [CrossRef] [PubMed]
25. Yadav, P.S.; Singh, M.; Vinayagam, R.; Shukla, P. Therapies and Delivery Systems for Diabetic Wound Care: Current Insights and Future Directions. *Front. Pharmacol.* **2025**, *16*, 1628252. [CrossRef] [PubMed]
26. Xiong, Y.; Knoedler, S.; Alfertshofer, M.; Kim, B.-S.; Jiang, D.; Liu, G.; Rinkevich, Y.; Mi, B. Mechanisms and Therapeutic Opportunities in Metabolic Aberrations of Diabetic Wounds: A Narrative Review. *Cell Death Dis.* **2025**, *16*, 341. [CrossRef] [PubMed]
27. Li, R.; Xia, Z.; Li, B.; Tian, Y.; Zhang, G.; Li, M.; Dong, J. Advances in Supercritical Carbon Dioxide Extraction of Bioactive Substances from Different Parts of *Ginkgo biloba* L. *Molecules* **2021**, *26*, 4011. [CrossRef] [PubMed]
28. Ye, W.; Wang, J.; Little, P.J.; Zou, J.; Zheng, Z.; Lu, J.; Yin, Y.; Liu, H.; Zhang, D.; Liu, P.; et al. Anti-Atherosclerotic Effects and Molecular Targets of Ginkgolide B from *Ginkgo biloba*. *Acta Pharm. Sin. B* **2024**, *14*, 1–19. [CrossRef] [PubMed]
29. Wang, Y.-Y.; Li, R.-H.; Sun, X.; Xia, Z.-M.; Zhang, G.-J.; Li, B.; Tian, Y.; Li, M.; Liu, S.-C. Comparative Analysis of Phytochemical Constituents of *Ginkgo biloba* Flowers and Leaves, and Evaluation of Their Biological Activities. *Fitoterapia* **2025**, *185*, 106673. [CrossRef] [PubMed]
30. Wang, Y.-Y.; Li, R.-H.; Zhang, G.-J.; Xia, Z.-M.; Li, B.; Li, M.; Liu, S.-C. The Whole Ginkgo Resource: Flowers, Seeds, Leaves, Branches, and Trees—A Comprehensive Review of Their Active Ingredients, Pharmacology, and Applications. *Chem. Biodivers.* **2025**, *22*, e00485. [CrossRef] [PubMed]
31. Li, M.; Li, B.; Hou, Y.; Tian, Y.; Chen, L.; Liu, S.; Zhang, N.; Dong, J. Anti-Inflammatory Effects of Chemical Components from *Ginkgo biloba* L. Male Flowers on Lipopolysaccharide-Stimulated RAW264.7 Macrophages. *Phytother. Res.* **2019**, *33*, 989–997. [CrossRef] [PubMed]
32. Cruz, T.M.; Lima, A.S.; Zhou, F.; Zhang, L.; Azevedo, L.; Marques, M.B.; Granato, D. Bioaccessibility of Bioactive Compounds from *Pereskia aculeata* and Their Cellular Antioxidant Effect. *Food Chem.* **2024**, *460*, 140484. [CrossRef] [PubMed]
33. Alarcon-Gil, J.; Sierra-Magro, A.; Morales-Garcia, J.A.; Sanz-SanCristobal, M.; Alonso-Gil, S.; Cortes-Canteli, M.; Niso-Santano, M.; Martínez-Chacón, G.; Fuentes, J.M.; Santos, A.; et al. Neuroprotective and Anti-Inflammatory Effects of Linoleic Acid in Models of Parkinson's Disease: The Implication of Lipid Droplets and Lipophagy. *Cells* **2022**, *11*, 2297. [CrossRef] [PubMed]
34. Sala-Vila, A.; Fleming, J.; Kris-Etherton, P.; Ros, E. Impact of α-Linolenic Acid, the Vegetable ω-3 Fatty Acid, on Cardiovascular Disease and Cognition. *Adv. Nutr.* **2022**, *13*, 1584–1602. [CrossRef] [PubMed]
35. Arya, S.S.; Salve, A.R.; Chauhan, S. Peanuts as Functional Food: A Review. *J. Food Sci. Technol.* **2016**, *53*, 31–41. Erratum in: *J. Food Sci. Technol.* **2024**, *61*, 2222. https://doi.org/10.1007/s13197-015-2007-9. [PubMed]
36. Li, M. Chemical Constituents from the Male Flowers of *Ginkgo biloba* L. and Their Biological Activities. Ph.D. Thesis, Beijing Institute of Radiation Medicine, Beijing, China, 2019.
37. Ahmed, F.; Ahmed, A.; Tamoor, T.; Hassan, T. Comment on "Dual-Band Perfect Metamaterial Absorber Based on an Asymmetric H-Shaped Structure for Terahertz Waves [Materials] (2018) [2193; https://doi.org/10.3390/ma11112193]". *Materials* **2019**, *12*, 3914. [CrossRef] [PubMed]
38. Berry, C.E.; Kendig, C.B.; An, N.; Fazilat, A.Z.; Churukian, A.A.; Griffin, M.; Pan, P.M.; Longaker, M.T.; Dixon, S.J.; Wan, D.C. Role of Ferroptosis in Radiation-Induced Soft Tissue Injury. *Cell Death Discov.* **2024**, *10*, 313. [CrossRef] [PubMed]
39. Zhang, Y.; Zhu, S.; Gu, Y.; Feng, Y.; Gao, B. Network Pharmacology Combined with Experimental Validation to Investigate the Mechanism of the Anti-Hyperuricemia Action of Portulaca Oleracea Extract. *Nutrients* **2024**, *16*, 3549. [CrossRef] [PubMed]
40. Liu, L.; Wang, Y.; Zhang, J.; Wang, S. Advances in the Chemical Constituents and Chemical Analysis of *Ginkgo biloba* Leaf, Extract, and Phytopharmaceuticals. *J. Pharm. Biomed. Anal.* **2021**, *193*, 113704. [CrossRef] [PubMed]
41. Sawada, Y.; Akiyama, K.; Sakata, A.; Kuwahara, A.; Otsuki, H.; Sakurai, T.; Saito, K.; Hirai, M.Y. Widely Targeted Metabolomics Based on Large-Scale MS/MS Data for Elucidating Metabolite Accumulation Patterns in Plants. *Plant Cell Physiol.* **2009**, *50*, 37–47. [CrossRef] [PubMed]
42. Repert, S.; Matthes, S.; Rozhon, W. Quantification of Arbutin in Cosmetics, Drugs and Food Supplements by Hydrophilic-Interaction Chromatography. *Molecules* **2022**, *27*, 5673. [CrossRef] [PubMed]
43. Roman, M.C.; Betz, J.M.; Hildreth, J. Determination of Synephrine in Bitter Orange Raw Materials, Extracts, and Dietary Supplements by Liquid Chromatography with Ultraviolet Detection: Single-Laboratory Validation. *J. AOAC Int.* **2007**, *90*, 68–81. [CrossRef]
44. Wada, K.; Ishigaki, S.; Ueda, K.; Sakata, M.; Haga, M. An Antivitamin B6, 4′-Methoxypyridoxine, from the Seed of *Ginkgo biloba* L. *Chem. Pharm. Bull.* **1985**, *33*, 3555–3557. [CrossRef] [PubMed]
45. Kumar, R.; Murugananthan, G.; Nandakumar, K.; Talwar, S. Isolation of Anxiolytic Principle from Ethanolic Root Extract of *Cardiospermum halicacabum*. *Phytomedicine* **2011**, *18*, 219–223. [CrossRef] [PubMed]
46. Yu, J.; Liu, H.; Xiong, J.; Qu, S.; Xie, X.; Zhao, H.; Zhu, Z.; Wang, Y.; Han, Y. Non-Target Metabolomics Unravels the Effect and Mechanism of Lianpu Drink on Spleen-Stomach Damp-Heat Syndrome. *J. Chromatogr. B* **2024**, *1246*, 124281. [CrossRef] [PubMed]

47. Njoya, E.M.; McGaw, L.J.; Makhafola, T.J. Investigating the Phytochemical Composition, Antioxidant, and Anti-Inflammatory Potentials of *Cassinopsis ilicifolia* (Hochst.) Kuntze Extract against Some Oxidative Stress and Inflammation Molecular Markers. *Curr. Issues Mol. Biol.* **2024**, *46*, 9639–9658. [CrossRef] [PubMed]
48. Tawaha, K.; Sadi, R.; Qa'dan, F.; Matalka, K.Z.; Nahrstedt, A. A Bioactive Prodelphinidin from Mangifera Indica Leaf Extract. *Z. Für Naturforschung C* **2010**, *65*, 322–326. [CrossRef] [PubMed]
49. Dou, M.; Huang, J.; Yu, M.; Li, H.; Song, Y.; Peng, Z.; Du, S.; Bai, J. HPLC Combined with Chemometrics for Quality Control of Huamoyan Granules or Capsules. *Chin. Herb. Med.* **2024**, *16*, 449–456. [CrossRef] [PubMed]
50. Kaunda, J.S.; Liu, J.; Xu, Y.; Chen, Y.; Yue, C.; Zhang, X.; Zhang, R.; Amin, M.; Xiao, W.; Li, H.; et al. Constituents from Leaves of *Macaranga hemsleyana*. *Chin. Herb. Med.* **2024**, *16*, 481–486. [CrossRef] [PubMed]
51. He, Y.; Wu, F.; Tan, Z.; Zhang, M.; Li, T.; Zhang, A.; Miao, J.; Ou, M.; Long, L.; Sun, H.; et al. Quality Markers' Discovery and Quality Evaluation of Jigucao Capsule Using UPLC-MS/MS Method. *Molecules* **2023**, *28*, 2494. [CrossRef] [PubMed]
52. Kim, S.; Thiessen, P.A.; Bolton, E.E.; Chen, J.; Fu, G.; Gindulyte, A.; Han, L.; He, J.; He, S.; Shoemaker, B.A.; et al. PubChem Substance and Compound Databases. *Nucleic Acids Res.* **2016**, *44*, D1202–D1213. [CrossRef] [PubMed]
53. Chen, X.; Kong, L.; Sheng, L.; Li, X.; Zou, H. Applications of Two-Dimensional Liquid Chromatography Coupled to Mass Spectrometry for the Separation and Identification of Compounds in *Ginkgo biloba* Extracts. *Se Pu Chin. J. Chromatogr.* **2005**, *23*, 46–51.
54. Xu, F.; Li, L.; Zhang, W.; Cheng, H.; Sun, N.; Cheng, S.; Wang, Y. Isolation, Characterization, and Function Analysis of a Flavonol Synthase Gene from *Ginkgo biloba*. *Mol. Biol. Rep.* **2012**, *39*, 2285–2296. [CrossRef] [PubMed]
55. Biernacka, P.; Felisiak, K.; Adamska, I. The Potential of Dried *Ginkgo biloba* Leaves as a Novel Ingredient in Fermented Beverages of Enhanced Flavour and Antioxidant Properties. *Food Chem.* **2024**, *461*, 141018. [CrossRef] [PubMed]
56. Gao, S.; Wang, J.; Cheng, L.; Fan, Y.; Qin, W.; Wang, Y.; Guo, Y.; Zhang, X.; Yang, Y. Evaluation of the Effects of Processing Technique on Chemical Components in Raphani Semen by HPLC and UPLC-Q-TOF-MS. *Int. J. Anal. Chem.* **2022**, *2022*, 8279839. [CrossRef] [PubMed]
57. Ellnain-Wojtaszek, M.; Zgórka, G. HIGH-PERFORMANCE LIQUID CHROMATOGRAPHY AND THIN-LAYER CHROMATOGRAPHY OF PHENOLIC ACIDS FROM *Ginkgo biloba* L. LEAVES COLLECTED WITHIN VEGETATIVE PERIOD. *J. Liq. Chromatogr. Relat. Technol.* **1999**, *22*, 1457–1471. [CrossRef]
58. Wu, J.; Huang, H.; Gong, L.; Tian, X.; Peng, Z.; Zhu, Y.; Wang, W. A Flavonoid Glycoside Compound from *Siraitia grosvenorii* with Anti-Inflammatory and Hepatoprotective Effects In Vitro. *Biomolecules* **2024**, *14*, 450. [CrossRef] [PubMed]
59. Wang, H.; Zeng, L.; Ding, H. A Novel Strategy for Screening of Secondary Metabolites in *Ginkgo biloba* Leaves by Ultra-Performance Liquid Chromatography–Tandem Information Dependent Acquisition Mass Spectrometry. *J. Anal. Chem.* **2024**, *79*, 330–338. [CrossRef]
60. Baker, T.R.; Regg, B.T. A Multi-Detector Chromatographic Approach for Characterization and Quantitation of Botanical Constituents to Enable in Silico Safety Assessments. *Anal. Bioanal. Chem.* **2018**, *410*, 5143. [CrossRef] [PubMed]
61. Meenu, M.; Kaur, S.; Yadav, M.; Sharma, A.; Tiwari, V.; Ali, U.; Giri, L.; Badwal, A.K.; Garg, M. Impact of Inherent Chemical Composition of Wheat and Various Processing Technologies on Whole Wheat Flour and Its Final Products. *Cereal Res. Commun.* **2024**, *53*, 409–424. [CrossRef]
62. Shirai, M.; Kawai, Y.; Yamanishi, R.; Terao, J. Approach to Novel Functional Foods for Stress Control 5. Antioxidant Activity Profiles of Antidepressant Herbs and Their Active Components. *J. Med. Investig.* **2005**, *52*, 249–251. [CrossRef] [PubMed]
63. Zhang, F.; Fei, Q.; Huang, X.; Yu, S.; Qiu, R.; Guan, L.; Wu, B.; Shan, M. LC-MS Based Strategy for Chemical Profiling and Quantification of Dispensing Granules of *Ginkgo biloba* Seeds. *Heliyon* **2024**, *10*, e36909. [CrossRef] [PubMed]
64. Sun, Y.; Wang, L.; Du, L.; Yu, H.; Tian, Y.; Jin, H.; Li, S.; Yan, S.; Xiao, X. Investigation on the Mechanism of Ginkgo Folium in the Treatment of Non-Alcoholic Fatty Liver Disease by Strategy of Network Pharmacology and Molecular Docking. *Technol. Health Care* **2023**, *31*, 209–221. [CrossRef] [PubMed]
65. Lee, D.; Yu, J.S.; Huang, P.; Qader, M.; Manavalan, A.; Wu, X.; Kim, J.-C.; Pang, C.; Cao, S.; Kang, K.S.; et al. Identification of Anti-Inflammatory Compounds from Hawaiian Noni (*Morinda citrifolia* L.) Fruit Juice. *Molecules* **2020**, *25*, 4968. [CrossRef] [PubMed]
66. Zhou, K.; Xiao, S.; Cao, S.; Zhao, C.; Zhang, M.; Fu, Y. Improvement of Glucolipid Metabolism and Oxidative Stress via Modulating PI3K/Akt Pathway in Insulin Resistance HepG2 Cells by Chickpea Flavonoids. *Food Chem. X* **2024**, *23*, 101630. [CrossRef] [PubMed]
67. Alruwad, M.I.; El Dine, R.S.; Gendy, A.M.; Saleh, A.M.; Khalaf, M.A.; El Hefnawy, H.M.; Sabry, M.M. Insights into *Clematis cirrhosa* L. Ethanol Extract: Cytotoxic Effects, LC-ESI-QTOF-MS/MS Chemical Profiling, Molecular Docking, and Acute Toxicity Study. *Pharmaceuticals* **2024**, *17*, 1347. [CrossRef] [PubMed]
68. Bampali, E.; Germer, S.; Bauer, R.; Kulić, Ž. HPLC-UV/HRMS Methods for the Unambiguous Detection of Adulterations of *Ginkgo biloba* Leaves with Sophora Japonica Fruits on an Extract Level. *Pharm. Biol.* **2021**, *59*, 436. [CrossRef] [PubMed]

69. Jiao, H.; Guan, Q.; Dong, R.; Ran, K.; Wang, H.; Dong, X.; Wei, S. Metabolomics Analysis of Phenolic Composition and Content in Five Pear Cultivars Leaves. *Plants* **2024**, *13*, 2513. [CrossRef] [PubMed]
70. Penna-Coutinho, J.; Aguiar, A.C.; Krettli/, A.U. Commercial Drugs Containing Flavonoids Are Active in Mice with Malaria and in Vitro against Chloroquine-Resistant Plasmodium Falciparum. *Mem. Inst. Oswaldo Cruz* **2018**, *113*, e180279. [CrossRef] [PubMed]
71. Hasler, A.; Gross, G.A.; Meier, B.; Sticher, O. Complex Flavonol Glycosides from the Leaves of *Ginkgo biloba*. *Phytochemistry* **1992**, *31*, 1391–1394. [CrossRef] [PubMed]
72. Ma, B.; Wang, S.; Li, H.; Wang, Q.; Hong, Y.; Bao, Y.-M.; Liu, H.; Li, M.; Zhao, Y.; Guo, L.-P. Combining Metabolomics and Transcriptomics to Reveal the Potential Medicinal Value of Rare Species Glycyrrhiza Squamulose. *Heliyon* **2024**, *10*, e30868. [CrossRef] [PubMed]
73. Zhang, X.; Yu, X.; Sun, X.; Meng, X.; Fan, J.; Zhang, F.; Zhang, Y. Comparative Study on Chemical Constituents of Different Medicinal Parts of *Lonicera japonica* Thunb. Based on LC-MS Combined with Multivariate Statistical Analysis. *Heliyon* **2024**, *10*, e31722. [CrossRef] [PubMed]
74. Aoki, D.; Hanaya, Y.; Akita, T.; Matsushita, Y.; Yoshida, M.; Kuroda, K.; Yagami, S.; Takama, R.; Fukushima, K. Distribution of Coniferin in Freeze-Fixed Stem of *Ginkgo biloba* L. by Cryo-TOF-SIMS/SEM. *Sci. Rep.* **2016**, *6*, 31525. [CrossRef] [PubMed]
75. Zhu, T.; Wang, L.; Feng, Y.; Sun, G.; Sun, X. Classical Active Ingredients and Extracts of Chinese Herbal Medicines: Pharmacokinetics, Pharmacodynamics, and Molecular Mechanisms for Ischemic Stroke. *Oxidative Med. Cell. Longev.* **2021**, *2021*, 8868941. [CrossRef] [PubMed]
76. Otsuka, H.; Zhong, X.N.; Hirata, E.; Shinzato, T.; Takeda, Y. Myrsinionosides A-E: Megastigmane Glycosides from the Leaves of *Myrsine seguinii* Lev. *Chem. Pharm. Bull.* **2001**, *49*, 1093–1097. [CrossRef] [PubMed]
77. Kim, J.A.; Yang, S.Y.; Wamiru, A.; McMahon, J.B.; Le Grice, S.F.J.; Beutler, J.A.; Kim, Y.H. New Monoterpene Glycosides and Phenolic Compounds from *Distylium racemosum* and Their Inhibitory Activity against Ribonuclease H. *Bioorganic Med. Chem. Lett.* **2011**, *21*, 2840–2844. [CrossRef] [PubMed]
78. Lephatsi, M.M.; Choene, M.S.; Kappo, A.P.; Madala, N.E.; Tugizimana, F. An Integrated Molecular Networking and Docking Approach to Characterize the Metabolome of *Helichrysum splendidum* and Its Pharmaceutical Potentials. *Metabolites* **2023**, *13*, 1104. [CrossRef] [PubMed]
79. Yang, T.; Deng, F.; Yang, X.; Li, S. Establishment of HPLC Fingerprints for Feiqizhong Tablets and Simultaneous Determination of Fourteen Constituents. *J. Anal. Methods Chem.* **2024**, *2024*, 7703951. [CrossRef] [PubMed]
80. Wang, Y.; Jia, M.; Gao, Y.; Zhao, B. Multiplex Quantitative Analysis of 9 Compounds of Scutellaria Baicalensis Georgi in the Plasma of Respiratory Syncytial Virus-Infected Mice Based on HPLC-MS/MS and Pharmacodynamic Effect Correlation Analysis. *Molecules* **2023**, *28*, 6001. [CrossRef] [PubMed]
81. Qiu, J.; Chen, X.; Netrusov, A.I.; Zhou, Q.; Guo, D.; Liu, X.; He, H.; Xin, X.; Wang, Y.; Chen, L. Screening and Identifying Antioxidative Components in *Ginkgo biloba* Pollen by DPPH-HPLC-PAD Coupled with HPLC-ESI-MS2. *PLoS ONE* **2017**, *12*, e0170141. [CrossRef] [PubMed]
82. Muchiri, R.N.; van Breemen, R.B. Chemical Standardization of Milk Thistle (*Silybum marianum* L.) Extract Using UHPLC-MS/MS and the Method of Standard Addition. *J. Am. Soc. Mass. Spectrom.* **2024**, *35*, 1726–1732. [CrossRef] [PubMed]
83. Ni, J.; Zhang, N.; Zhan, Y.; Ding, K.; Qi, P.; Wang, X.; Ding, W.; Xu, M. Transgenic Tobacco Plant Overexpressing Ginkgo Dihydroflavonol 4-Reductase Gene GbDFR6 Exhibits Multiple Developmental Defects. *Front. Plant Sci.* **2022**, *13*, 1066736. [CrossRef] [PubMed]
84. Mao, R.; Bai, Z.; Wu, J.; Han, R.; Zhang, X.; Chai, W.; Liang, Z. Transcriptome and HPLC Analysis Reveal the Regulatory Mechanisms of Aurantio-Obtusin in Space Environment-Induced *Senna obtusifolia* Lines. *Int. J. Environ. Res. Public Health* **2022**, *19*, 898. [CrossRef] [PubMed]
85. Hyun, S.K.; Kang, S.S.; Son, K.H.; Chung, H.Y.; Choi, J.S. Biflavone Glucosides from *Ginkgo biloba* Yellow Leaves. *Chem. Pharm. Bull.* **2005**, *53*, 1200–1201. [CrossRef] [PubMed]
86. Zhang, Q.; Wang, G.; A, J.; Wu, D.; Zhu, L.; Ma, B.; Du, Y. Application of GC/MS-Based Metabonomic Profiling in Studying the Lipid-Regulating Effects of *Ginkgo biloba* Extract on Diet-Induced Hyperlipidemia in Rats. *Acta Pharmacol. Sin.* **2009**, *30*, 1674–1687. [CrossRef] [PubMed]
87. Qazi, S.S.; Lombardo, D.A.; Abou-Zaid, M.M. A Metabolomic and HPLC-MS/MS Analysis of the Foliar Phenolics, Flavonoids and Coumarins of the Fraxinus Species Resistant and Susceptible to Emerald Ash Borer. *Molecules* **2018**, *23*, 2734. [CrossRef] [PubMed]
88. Bouzenad, N.; Ammouchi, N.; Chaib, N.; Messaoudi, M.; Bousabaa, W.; Bensouici, C.; Sawicka, B.; Atanassova, M.; Ahmad, S.F.; Zahnit, W. Exploring Bioactive Components and Assessing Antioxidant and Antibacterial Activities in Five Seaweed Extracts from the Northeastern Coast of Algeria. *Mar. Drugs* **2024**, *22*, 273. [CrossRef] [PubMed]
89. Chen, Q.-L.; Shi, Z.-Y.; Zhang, Y.-H.; Zheng, J.-B. Study on the Chemical Constituents in Roots of Gentiana Dahurica. *Zhong Yao Cai* **2011**, *34*, 1214–1216. [PubMed]

90. Alves, O.J.A.; Ozelin, S.D.; Magalhães, L.F.; Candido, A.C.B.B.; Gimenez, V.M.M.; Silva, M.L.A.E.; Cunha, W.R.; Januário, A.H.; Tavares, D.C.; Magalhães, L.G.; et al. HPLC Method for Quantifying Verbascoside in *Stizophyllum perforatum* and Assessment of Verbascoside Acute Toxicity and Antileishmanial Activity. *Front. Plant Sci.* **2023**, *14*, 1324680. [CrossRef] [PubMed]
91. Ouyang, Y.; Su, X.; Zheng, X.; Zhang, L.; Chen, Z.; Yan, Q.; Qian, Q.; Zhao, J.; Li, P.; Wang, S. Mussel-Inspired "All-in-One" Sodium Alginate/Carboxymethyl Chitosan Hydrogel Patch Promotes Healing of Infected Wound. *Int. J. Biol. Macromol.* **2024**, *261*, 129828. [CrossRef] [PubMed]
92. Wang, J.; Wang, Y.; Huang, R.; Li, W.; Fan, W.; Hu, X.; Yang, X.; Han, Q.; Wang, H.; Liu, G. Uncovering the Pharmacological Mechanisms of Zizhu Ointment against Diabetic Ulcer by Integrating Network Analysis and Experimental Evaluation in Vivo and in Vitro. *Front. Pharmacol.* **2022**, *13*, 1027677. [CrossRef] [PubMed]
93. Burgess, J.L.; Wyant, W.A.; Abdo Abujamra, B.; Kirsner, R.S.; Jozic, I. Diabetic Wound-Healing Science. *Medicina* **2021**, *57*, 1072. [CrossRef] [PubMed]
94. Wang, M.; Wang, X. Dynamic Regulation of the Wound Repair Process: Achieving One-Stop Scar-Free Repair. *Biomater. Transl.* **2024**, *5*, 200–202. [CrossRef] [PubMed]
95. Littig, J.P.B.; Moellmer, R.; Estes, A.M.; Agrawal, D.K.; Rai, V. Increased Population of CD40+ Fibroblasts Is Associated with Impaired Wound Healing and Chronic Inflammation in Diabetic Foot Ulcers. *J. Clin. Med.* **2022**, *11*, 6335. [CrossRef] [PubMed]
96. Wang, M.; Cao, X.; Shang, Y.; Jiang, Y.; Chen, P.; Duan, C.; Zhang, D.; Wang, P.; Ji, J.; Gong, Z. Correlational Analysis of PLIN1 with Inflammation in Diabetic Foot Ulcer Wounds. *Diabetes Res. Clin. Pract.* **2024**, *209*, 111605. [CrossRef] [PubMed]
97. Yan, Z.; Zhang, Y.; Chen, Q.; Li, J.; Ning, X.; Bai, F.; Wang, Y.; Liu, X.; Liu, Y.; Zhang, M.; et al. Carbon Dot Superoxide Dismutase Nanozyme Enhances Reactive Oxygen Species Scavenging in Diabetic Skin Wound Repair. *J. Adv. Res.* **2026**, *79*, 691–706. [CrossRef] [PubMed]
98. Huang, Y.; Ding, Y.; Ma, Z.; Yang, P.; Ding, X.; Yan, X. Omentin-1 Promotes Wound Healing in Diabetic Mice by Improving Vascular Endothelial Cell Function. *Sci. Rep.* **2025**, *15*, 40956. [CrossRef] [PubMed]
99. Cao, G.; Yin, S.; Ma, J.; Lu, Y.; Song, R.; Wu, Z.; Liu, C.; Liu, J.; Wu, P.; Sun, R.; et al. YAP Promotes the Healing of Ischemic Wounds by Reducing Ferroptosis in Skin Fibroblasts through Inhibition of Ferritinophagy. *Heliyon* **2024**, *10*, e24602. [CrossRef] [PubMed]
100. Geng, X.; Wang, Y.; Li, H.; Song, L.; Luo, C.; Gu, X.; Zhong, H.; Chen, H.; Chen, X.; Wang, J.; et al. Total Iridoid Glycoside Extract of *Lamiophlomis rotata* (Benth) Kudo Accelerates Diabetic Wound Healing by the NRF2/COX2 Axis. *Chin. Med.* **2024**, *19*, 53. [CrossRef] [PubMed]
101. Lin, Z.; Li, L.-Y.; Chen, L.; Jin, C.; Li, Y.; Yang, L.; Li, C.-Z.; Qi, C.-Y.; Gan, Y.-Y.; Zhang, J.-R.; et al. Lonicerin Promotes Wound Healing in Diabetic Rats by Enhancing Blood Vessel Regeneration through Sirt1-Mediated Autophagy. *Acta Pharmacol. Sin.* **2024**, *45*, 815–830. [CrossRef] [PubMed]
102. Liu, Y.; Xin, H.; Zhang, Y.; Che, F.; Shen, N.; Cui, Y. Leaves, Seeds and Exocarp of *Ginkgo biloba* L. (Ginkgoaceae): A Comprehensive Review of Traditional Uses, Phytochemistry, Pharmacology, Resource Utilization and Toxicity. *J. Ethnopharmacol.* **2022**, *298*, 115645. [CrossRef] [PubMed]
103. Li, R.; Wang, Y.; Sun, X.; Xia, Z.; Tian, Y.; Chen, B.; Liu, S.; Li, M.; Yan, X. Active Components of *Ginkgo biloba* Flower Attenuate Radiation-Induced Cognitive Impairment via Inhibiting Ferroptosis. *Antioxidants* **2026**, *15*, 183. [CrossRef] [PubMed]
104. Li, Q.; Ye, T.; Long, T.; Peng, X. Ginkgetin Exerts Anti-Inflammatory Effects on Cerebral Ischemia/Reperfusion-Induced Injury in a Rat Model via the TLR4/NF-κB Signaling Pathway. *Biosci. Biotechnol. Biochem.* **2019**, *83*, 675–683. [CrossRef] [PubMed]
105. Lv, Y.; Weng, X.; Zhu, Y.; Zhang, X.; Ma, Y.; Dai, X.; Bai, X.; Zhang, S.; Qi, J.; Zhu, X.; et al. Quercetin Alleviates Postmenopausal Atherosclerosis by Suppressing Endothelial Cell Ferroptosis via Regulating the KEAP1/NRF2/GPX4 Signalling Pathway. *Br. J. Pharmacol.* **2026**, *183*, 620–643. [CrossRef] [PubMed]
106. Chen, J.; Ou, Z.; Gao, T.; Yang, Y.; Shu, A.; Xu, H.; Chen, Y.; Lv, Z. Ginkgolide B Alleviates Oxidative Stress and Ferroptosis by Inhibiting GPX4 Ubiquitination to Improve Diabetic Nephropathy. *Biomed. Pharmacother.* **2022**, *156*, 113953. [CrossRef] [PubMed]
107. Pang, T.; Shao, Y.; Zhou, L.; Wang, Z.; Xi, P.; Zhang, Y.; Xie, L.; Deng, Z. rhaFGF Promotes Acute Diabetic Wound Healing by Suppressing Chronicity of Inflammation. *Sci. Rep.* **2025**, *15*, 19085. [CrossRef] [PubMed]
108. Wang, Y.; Liang, J.; Chen, Y.; Tian, T.; Ma, W.; Liu, Z.; Tang, B.; Wang, R.; He, Y.; Zhang, T.; et al. DNA Tetrahedron Functionalized Microneedles Blocking IL-6 to Promote Skin Wound Healing. *ACS Appl. Mater. Interfaces* **2025**, *17*, 42717–42734. [CrossRef] [PubMed]
109. The Antioxidant Glutathione. In *Vitamins and Hormones*; Academic Press: Cambridge, MA, USA, 2023; Volume 121, pp. 109–141.
110. Zheng, J.; Zhang, W.; Ito, J.; Henkelmann, B.; Xu, C.; Mishima, E.; Conrad, M. N-Acetyl-l-Cysteine Averts Ferroptosis by Fostering Glutathione Peroxidase 4. *Cell Chem. Biol.* **2025**, *32*, 767–775.e5. [CrossRef] [PubMed]
111. Iásly, L.C.; Adjafre, B.L.; Sousa, S.H.A.F.; Castro, R.R. Galactomannan of *Delonix regia* Seeds Modulates Cytokine Expression and Oxidative Stress Eliciting Anti-Inflammatory and Healing Effects in Mice Cutaneous Wound. *Int. J. Biol. Macromol.* **2022**, *203*, 342–349. [CrossRef] [PubMed]

112. Bersuker, K.; Hendricks, J.M.; Li, Z.; Magtanong, L.; Ford, B.; Tang, P.H.; Roberts, M.A.; Tong, B.; Maimone, T.J.; Zoncu, R.; et al. The CoQ Oxidoreductase FSP1 Acts Parallel to GPX4 to Inhibit Ferroptosis. *Nature* **2019**, *575*, 688–692. [CrossRef] [PubMed]
113. SharathBabu, B.N.; Shivangi, S.; Valiyaveettil, A.; Annaraj, B.; Mugesh, G. Small Molecule Selenium-Based Glutathione Peroxidase 4 Mimetic Inhibits Lipid Peroxidation and Protects Cultured Neurons from Ferroptosis. *Free. Radic. Biol. Med.* **2025**, *238*, 275–292. [CrossRef] [PubMed]
114. Wang, Y.-W.; Chen, T.C.-Y.; Luo, C.-W. Engineering a Single-Chain Vascular Endothelial Growth Factor with Enhanced Physiological Stability for Accelerating Wound Healing. *Int. J. Biol. Macromol.* **2025**, *321*, 146281. [CrossRef] [PubMed]
115. Belvedere, R.; Novizio, N.; Morello, S.; Petrella, A. The Combination of Mesoglycan and VEGF Promotes Skin Wound Repair by Enhancing the Activation of Endothelial Cells and Fibroblasts and Their Cross-Talk. *Sci. Rep.* **2022**, *12*, 11041. [CrossRef] [PubMed]
116. Li, S.; Li, Y.; Wu, Z.; Wu, Z.; Fang, H. Diabetic Ferroptosis Plays an Important Role in Triggering on Inflammation in Diabetic Wound. *Am. J. Physiol.-Endocrinol. Metab.* **2021**, *321*, E509–E520. [CrossRef] [PubMed]
117. Hirschhorn, T.; Stockwell, B.R. The Development of the Concept of Ferroptosis. *Free. Radic. Biol. Med.* **2019**, *133*, 130–143. [CrossRef] [PubMed]

Disclaimer/Publisher's Note: The statements, opinions and data contained in all publications are solely those of the individual author(s) and contributor(s) and not of MDPI and/or the editor(s). MDPI and/or the editor(s) disclaim responsibility for any injury to people or property resulting from any ideas, methods, instructions or products referred to in the content.